ABSTRACT

Discovery of Novel 3'-Phosphoadenosine-5'-Phosphosulfate (PAPS) Reductase from Methanarcheon *Methanocaldococcus jannaschii*

Myung Kook Cho, M.S.

Mentor: Sung-Kun Kim, Ph.D.

This study explores the potential assimilatory sulfate reduction pathway in methanarcheon by investigating the gene product of the open reading frame *Mj0066*. We expressed and purified the gene product of *Mj0066* of *Methanocaldococcus jannaschii* to explore its substrate specificity and the reaction kinetics. Kinetic studies revealed the wild-type enzyme specifically reduced PAPS with *E. coli* thioredoxin supplied as the electron donor. The K_m, V_{max}, and k_{cat}/K_m value was 15.9 μM, 0.09429 $\mu Mmg^{-1}min^{-1}$, and 5571 $M^{-1}s^{-1}$, respectively, at pH 8.0 and 30 ^oC. Therefore, the gene product of *Mj0066* was identified as a novel 5'-phosphoadenosine-phosphosulfate reductase. Furthermore, site directed mutagenesis of individual cysteines and redox titration were performed in order to investigate the catalytic mechanism. The combined studies show Cys337 plays a role in substrate binding while Cys19 and Cys22 are involved in electron transfer. Taken together, PAPS-reductase activity advocates the presence of a PAPS-utilizing assimilatory sulfate reduction pathway *M. jannaschii*.

Discovery of Novel 3'-Phosphoadenosine-5'-Phosphosulfate (PAPS) Reductase from Methanarcheon *Methanocaldococcus jannaschii*

by

Myung Kook Cho, B.A.

A Thesis

Department of Chemistry and Biochemistry

_____

Patrick J. Farmer, Ph.D., Chairperson

Submitted to the Graduate Faculty of
Baylor University in Partial Fulfillment of the
Requirements for the Degree
of

Master of Science

Approved by the Thesis Committee

_____

Sung-Kun Kim, Ph.D., Chairperson

_____

Bryan F. Shaw, Ph.D.

_____

Kenneth T. Park, Ph.D.

Accepted by the Graduate School

August 2013

_____

J. Larry Lyon, Ph.D., Dean

Page bearing signatures is kept on file in the Graduate School.

TABLE OF CONTENTS

LIST OF FIGURES

LIST OF TABLES

LIST OF ABBREVIATIONS

APR — Adenosine 5'-phosphosulfate reductase
APS — Adeonsine 5'-phosphosulfate
Asn — Asparagine
ATP — Adenosine triphosphate
CoB — Coenzyme B
CoM — Coenzyme M
Cys — Cysteine
DNA — Deoxyribonucleic acid
E. coli — *Escherichia coli*
EcPAPR — *Escherichia coli* PAPR
EDTA — Ethylenediaminetetraacetic acid
ESI-MS — Electrospray ionization mass spectrometry
Grx — Glutaredoxin
HEPES — 4-(2-hydroxyethyl)-1-piperazineethanesulfonic acid
H_4MPT — Tetrahydromethanopterin
IPTG — Isopropyl-beta-D-thioglactopyranoside
LB — Luria broth
LPLC — Low pressure liquid chromatography
MES — 2-(*N*-morpholino)ethanesulfonic acid
MFR – Methanofuran
Mj — *Methanocaldococcus jannaschii*
MjAPR — *Methanocaldococcus jannaschii* APR
MjPAPR — *Methanocaldococcus jannaschii* PAPR
NADPH — Nicotinamide adenine dinucleotide phosphate
NCBI — National Center for Biotechnology Information
ORF — Open reading frame
PAGE — Polyacrylamide gel electrophoresis
PAPR — 3'-phosphoadenosine-5'-phosphosulfate reductase
PAPS — 3'-phosphoadenosine-5'-phosphosulfate
PCR — Polyacrylamide gel electrophoresis
PDB — Protein data bank
RMSD — Root mean square
S. cerevisiae — *Saccharomyces cerevisiae*
ScPAPR — *Saccharomyces cerevisiae* PAPR
SDS — Sodium dodecyl sulfate
Thr — Threonine
Trx — Thioredoxin
Tyr — Tyrosine
UV — Ultraviolet
VIS — Visible

ACKNOWLEDGEMENTS

I would like to thank Dr. Sung-Kun Kim and Jong-sun Lee for the project and being my mentors. I would also like to thank my parents for helping me, mentally, financially, emotionally, and spiritually, through this journey. Anytime I wanted to quit and leave, they were there to remind me I should finish what I started. They nurtured me through everything. I would like to thank my sister, Ahra, and her husband, Raymond Cheng, for their encouragement. Finally, I would like to thank God and all of his blessings.

CHAPTER ONE

Introduction

Sulfur is an essential element utilized by all living organisms for various purposes, such as biosynthesis of most sulfur-containing compounds or anaerobic energy source. Since sulfur naturally exists as sulfate (SO_4^{2-}) [1], it is necessary for organisms to reduce the sulfate into a non-oxyanion form, sulfide, which is used as their sole sulfur source [2, 3]. The sulfate metabolism in organisms such as bacteria, cyanobacteria, fungi, and plants incorporates a cascade of reduction processes, which reduce the inorganic sulfate (oxidation state +6) to sulfite (oxidation state +4) and then finally to sulfide (oxidation state -2) [2, 4, 5]. However, the redox potential of a direct reduction of sulfate to sulfite is unfavorably low ($E°'$=-517 mV) for a biological setting [6, 7]. For this reason, the sulfate is first required to be activated by coupling the sulfate to ATP in order to produce adenosine 5'-phosphosulfate (APS) or 3'-phosphoadenosine-5'-phosphosulfate (PAPS), thus increasing the reduction potential to a more biologically favorable potential [2]. The APS is reduced by an APS reductase (APR) that typically contains a [4Fe-4S] cluster [5, 8, 9]. In contrast, PAPS is reduced by PAPS reductase (PAPR), which is an enzyme that lacks cofactors or any other prosthetic groups [9, 10]. These sulfonucleotide reductases catalyze the reduction of adenylated sulfate to sulfite with the input of two electrons from thioredoxin (Trx) or glutaredoxin (Grx) [9]. Sulfite is further reduced to hydrogen sulfide, which can either be incorporated into organic compounds (assimilation) or released as a waste product (dissimilation) (Figure 1) [1, 5]. Sulfonucleotide reduction pathway utilizes two specific substrates for assimilation and dissimilation [18]. In the assimilatory

sulfonucleotide reduction pathway the enzyme PAPS-reductase has substrate specificity for 3'-phosphoadenosine-5'-phosphosulfate (PAPS), while the dissimilation pathway APS-reductase has specificity for 5'-adenophosphosulfate (APS) [18].

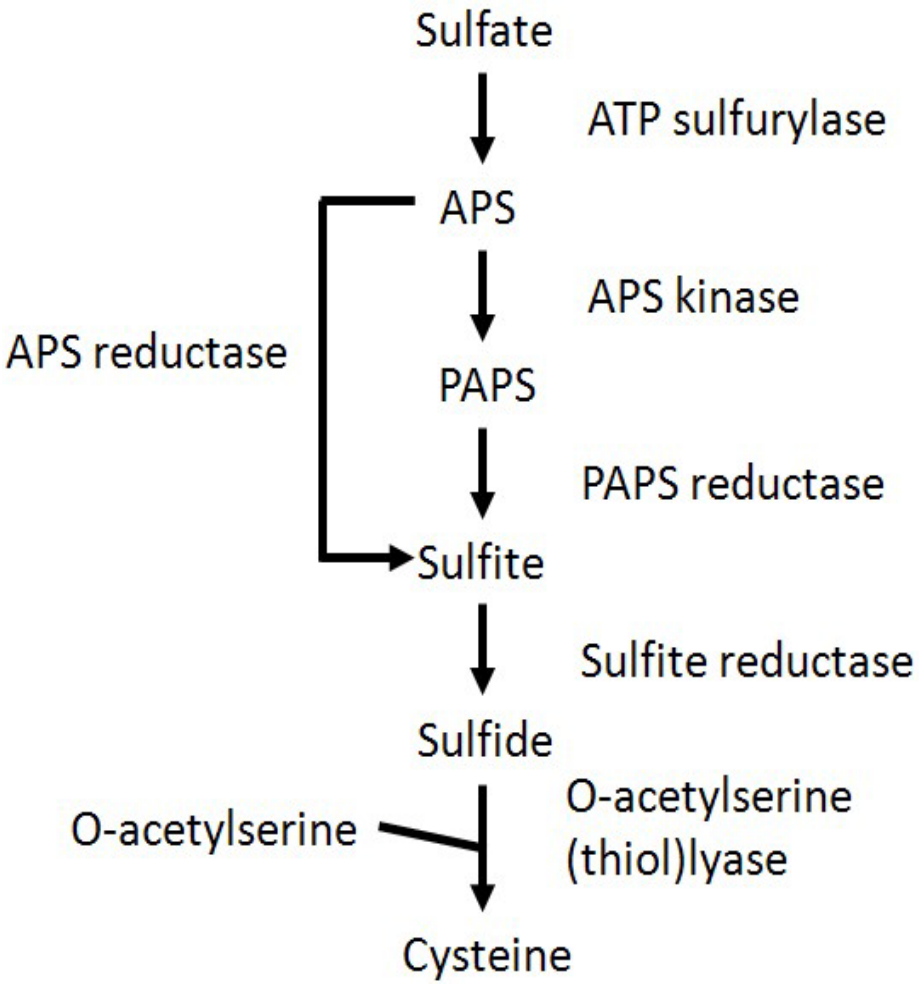

Figure 1. Sulfate reduction pathway. Sulfate is adenylated to APS with an input of ATP. The APS can be directly reduced to sulfite via APS-reductase (dissimilation) or APS can be further phosphorlayted by APS kinase into PAPS. The PAPS is then reduced to sulfite via PAPS-reductase (assimilation). The sulfite is further reduced to sulfide, which in assimilation can be incorporated into biological amino acids, such as cysteine, while dissimlation would excrete H_2S as a waste product.

Initially, the sulfate reduction pathway was expected to be absent in methanogens, such as *Methanocaldococcus jannaschii*, which is a hyperthermophilic, chemoautotroph that resides near deep-sea hydrothermal vents utilizing methanogenesis as a primary anaerobic energy source [3, 15]. Because sulfite, which is an intermediate of the sulfate reduction pathway, is an effective inhibitor of methyl coenzyme-M reductase (Figure 2) in methanogenesis, these two metabolic systems are presumably incompatible [11, 14]. However, the discovery of coenzyme F_{420} dependent sulfite reductase in *M. jannaschii* and other methyl-CoM reductase studies elucidated that there could be a viable resolution for the conflict between the two processes since the enzyme catalyzes the reduction of sulfite to sulfide without inhibiting methanogenesis [3, 11, 13, 14]. Other methanogens, such as *Methanobacterium thermoautotrophicum, Methanothermobacter thermautorophicus, Methanocaldococcus jannaschii,* and, *Methanococcus thermolithotrophicus*, has been reported to sustain growth with sulfite and sulfate as a sole sulfur source [16, 17]. Specifically, it has been reported that *Methanococcus thermolithotrophicus* is able to use sulfate as its sole sulfur source [16]. Also, we recently reported the novel discovery of an APS Reductase in *M. jannaschii* (MjAPR) [11], which has unique characteristics when compared to APRs from other organisms. Although MjAPR was highly conserved in the key regions of APRs (CCXXRKXXPL and SXGCXXCT), it shares little sequence similarity with other APRs [11]. MjAPR is further distinguished from other APRs with its lack of a [4Fe-4S] cluster. Instead, the MjAPR appears to incorporate a possible heme cofactor [11]. Therefore, this *M. jannaschii* likely possesses a possible sulfate metabolism pathway utilizing a novel APR [11] and sulfite reductase [3].

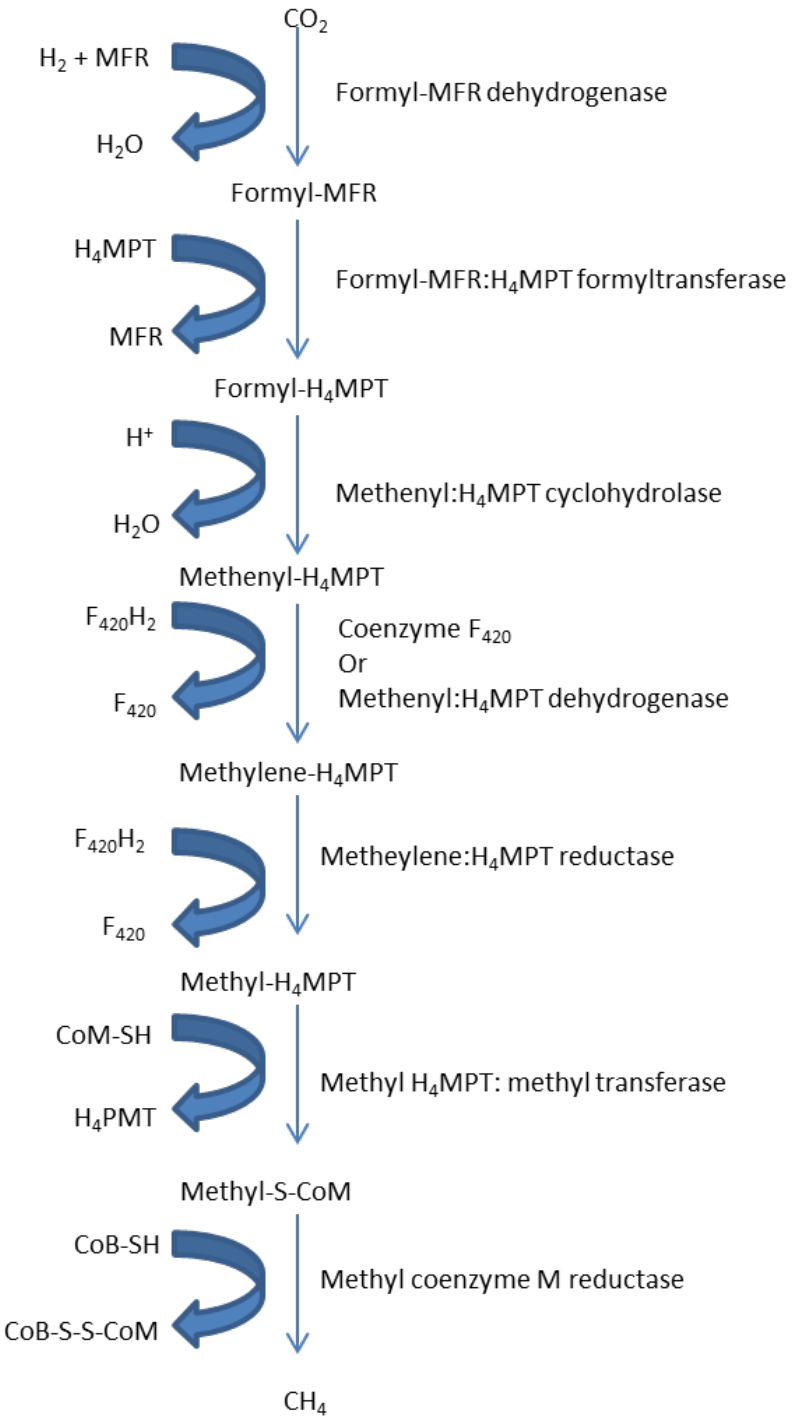

Figure 2. Methanogenesis pathway utilizing H_2 and CO_2 as the carbon source. The final product of methanogenesis is methane, which is produce by reduction of Methyl-S-CoM by Methyl-CoM reductase. Methyl-CoM reductase has been shown to be inhibited by sulfite, which is a produced in the sulfate reduction pathway (Modified from [14]).

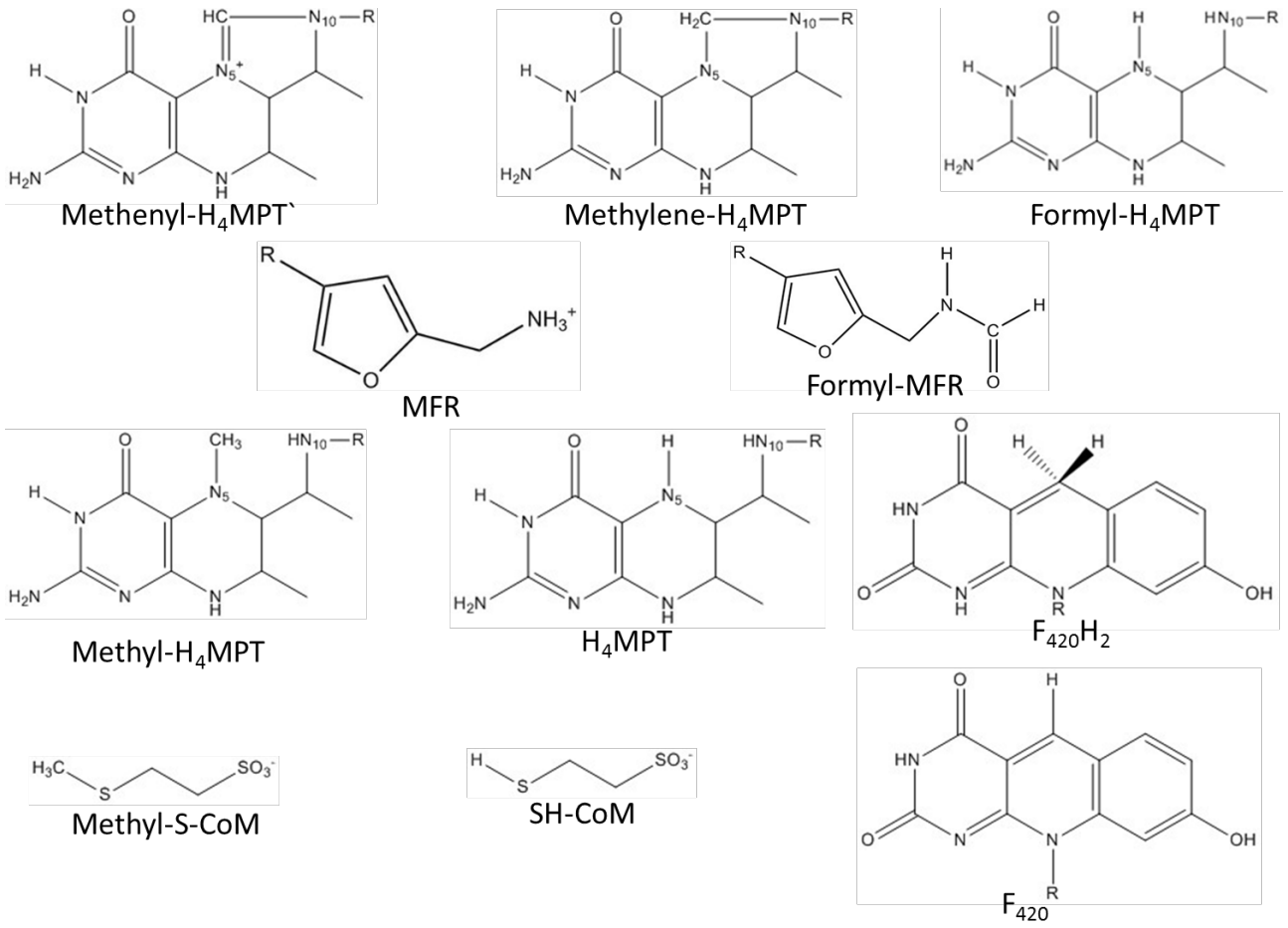

Figure 3. Structure of substrates and product of methanogenesis.

Interestingly, it has been promulgated that open reading frame (ORF) *Mj0066* evidently possessed several sequence similarities with PAPS-reductase [3, 12]. If *Mj0066* encodes a PAPS-reductase, *M. jannaschii* could potentially utilize the assimilatory sulfate reduction pathway instead of a dissimilatory sulfate reduction pathway [18]. A potential assimilatory sulfate reduction pathway seems more plausible because methanogens obtain energy through an anaerobic respiration method known as methanogenesis [13, 15, 17]. In order to investigate the possible utilization of PAPS in the sulfate reduction pathway of *M. jannaschii*, we examined the protein expressed by ORF *Mj0066* via spectroscopy and *in vitro* kinetic studies. In addition, a combination of amino acid sequence alignment, site-directed mutagenesis, and mass spectrometry analysis were used to gain insight into the reduction mechanism between substrate and enzyme. As described below, our study resulted in the first discovery of PAPR in methanarchaeon *M. jannaschii*, which suggests a possible assimilatory sulfate reduction pathway, while proposing a possible reduction mechanism of the PAPS within the organism.

CHAPTER TWO

Materials and Methods

Bioinformatics

The sequence analysis was conducted by aligning protein sequences *Methanocaldococcus jannaschii* (NP_247030), *Escherichia coli* (P17854) and *Saccharomyces cerevisiae* (P18408) obtained from NCBI sequence database (http://www.ncbi.nlm.nih.gov/) with BioEdit software.

Cloning of Mj0066

The *Mj0066* coding sequence from *M. jannaschii* genomic DNA was amplified by polymerase chain reaction (PCR) with *GoTaq*® DNA *Polymerase* (obtained from Promega) using the following PCR primers:

Forward: 5'- CACC ATG TGG GAA GTG ATA ATT ATG AAG ACA - 3'

Reverse: 5' - TTA TTG CCT TTT ATG TTT CCA TCT - 3'

The plasmid pET100::Mj0066 with six histidine codons at N-terminus was constructed using TOPO® cloning system as described in the manufacturer's instructions. The recombinant gene was used to transform *E. coli* strain BL21 (DE3) one shot competent cell (obtained from Invitrogen) for expression purposes. The *Mj0066* gene cloned in pET100 was identified by DNA sequencing.

Construction of Mj0066 Mutant Plasmids

To construct the mutant expression plasmids, a QuickChange site-directed mutagenesis kit (Stratagene) was employed according to the manufacturer's instructions. The plasmid pET100::Mj0066 was used as a template for the mutation of amino acids residue Cys19, Cys22, Cys31, Cys34, Cys337, Cys341, Cys425, and Cys428 to alanine. The nucleotide sequences of forward and reverse primers for mutations are listed in Table 1. The constructed mutant plasmids were transformed into XL1-Blue competent cells for screening purposes. The colonies with the mutant plasmids were identified by sequencing. The extracted mutant plasmids were then transformed into *E. coli* strain BL21 (DE3) competent cell for expression purposes.

Expression of the Recombinant Wild- Type and Mutant Proteins

The transformed *E. coli* strain BL21 (DE3) cells were grown at 37 ºC in 1 L of Luria-Bertani (LB) medium containing 50µg/ml ampicillin to an optical density of 0.6-0.7 (as measured using an eppendorf BioPhotometer plus), followed by induction with Isopropyl-beta-D-thiogalactopyranoside (IPTG) at a final concentration of 1.0 mM. After 6 h of induction and shaking at 30 ºC and 200 rpm, respectively, the cells were harvested by centrifugation at 4750 x g for 20 min at 4 ºC using a Beckman Coulter Allegra® X-15R centrifuge, and the cell pellets were stored at -80 ºC until use.

Purification of the Recombinant Wild- Type and Mutant Proteins

The cell pellets were resuspended in a buffer containing 200 mM NaCl, 1mM EDTA, and 30 mM Tris-HCl (pH 8.0). The cell suspension was French Pressed four times at a pressure of 12,000 psi, resulting in cell lysis. The cell lysate was centrifuged at

Table 1. Sequences of Oligonucleotide Primers Used in Site-Directed Mutagenesis PCR Amplification

Primer	Sequence 5'-3'													Mutated Codon
C19A For		ATA	CAT	TTA	AAA	TGG	**GCT**	AAA	AAT	TGT	AAT	GTC		TGT → GCT
C19A Rev		GAC	ATT	ACA	ATT	TTT	**AGC**	CCA	TTT	TAA	ATG	TAT		
C22A For	A	AAA	TGG	TGT	AAA	AAT	**GCT**	AAT	GTC	CCA	TTA	TTA	GGG	TGT → GCT
C22A Rev	CCC	TAA	TAA	TGG	GAC	ATT	**AGC**	ATT	TTT	ACA	CCA	TTT	T	
C31A For	CA	TTA	TTA	GGG	AGA	GTT	**GCT**	GAA	GTT	TGT	GGC	TCA	AA	TGT → GCT
C31A Rev	TT	TGA	GCC	ACA	AAC	TTC	**AGC**	AAC	TCT	CCC	TAA	TAA	TG	
C34A For	GG	AGA	GTT	TGT	GAA	GTT	**GCT**	GGC	TCA	AAA	GCT	G		TGT → GCT
C34A Rev		C	AGC	TTT	TGA	GCC	**AGC**	AAC	TTC	ACA	AAC	TCT	CC	
C337A For		AGA	GAT	TAT	AGA	TGG	**GCT**	TCT	GAA	ATC	TGT	AAG		TGT → GCT
C337A Rev		CTT	ACA	GAT	TTC	AGA	**AGC**	CCA	TCT	ATA	ATC	TCT		
C341A For		TGG	TGT	TCT	GAA	ATC	**GCT**	AAG	TTA	GAG	CCG	TTA		TGT → GCT
C341A Rev		TAA	CGG	CTC	TAA	CTT	**AGC**	GAT	TTC	AGA	ACA	CCA		
C425A For	A	TTT	GAT	AGG	ATT	GGC	**GCT**	TTT	ATG	TGT	CCA	GC		TGT → GCT
C425A Rev		GC	TGG	ACA	CAT	AAA	**AGC**	GCC	AAT	CCT	ATC	AAA	T	
C428A For		ATT	GGC	TGT	TTT	ATG	**GCT**	CCA	GCT	ATG	GAA	ATG		TGT → GCT
C428A Rev		CAT	TTC	CAT	AGC	TGG	**AGC**	CAT	AAA	ACA	GCC	AAT		

The altered codons are shown in boldface. For, forward; Rev, reverse.

25,000 x g for 20 min to remove insoluble cell debris. The supernatant was passed through a 0.45 micron filter for protein purification. The filtrate was loaded onto a Ni^{2+} affinity column (HisTrap™ HP purchased from GE Healthcare) attached to a BioRad BioLogic LP Liquid Chromatography System, which was pre-equilibrated with 20 ml Binding buffer (30 mM Tris-HCl (pH 8.0), 500 mM NaCl). After washing the column with Binding buffer containing 15 mM imidazole, the column was then eluted with a 60 ml linear gradient, which ranged from 15 - 250 mM imidazole in elution buffer containing 30 mM Tris-HCl (pH 8.0) and 500 mM NaCl, at a flow rate of 1 ml/min. The eluted fractions at the protein peak were collected at an imidazole concentration that approximately ranged between 150 mM and 200 mM. Using a Millipore Amicon Ultra-15 Centrifugal filter, collected fractions were concentrated and underwent two rounds of buffer exchange, thereby eliminating the imidazole and salt in the protein, respectively. Each exchange was done with 10 ml of a 30 mM Tris-HCl (pH 8.0) and 100 mM Na_2SO_4 buffer. The concentrated proteins in the same buffer were stored in 10% glycerol at -80 ºC. The purity of the proteins and their molecular mass were determined by SDS-PAGE on 12% gels, which were stained with Coomassie Brilliant Blue R-250. The protein concentrations were measured by UV-Vis analysis on a SHIMADZU UV-2450 UV-VIS spectrophotometer, using the Bradford method [13] with bovine serum albumin as a standard. The typical yields were approximately 4-5 mg of protein from 1 L of *E. coli* culture.

Enzymatic Assays

The APS Reductase and PAPS Reductase coupled-enzyme assays of the wild-type enzyme and its Cys/Ala variants were performed spectrophotometrically in the

presence of thioredoxin (Trx) and glutaredoxin (Grx) as electron donors. Reactions contained 100 mM Tris-HCl (pH 8.0), 1 mM EDTA (pH 8.0), 300 μM NADPH (Sigma-N 1630), 7 mM GSH or 1 mM Trx, 45 nM glutathione reductase (Sigma-G3664-100UN) or 1 μM NTR, and varying volumes of 5 mM APS (Sigma-N 1630) or 5 mM PAPS (Sigma-A 1651) in a volume of 1 mL. The Tris-HCl buffer was replaced with 50 mM MES, 50 mM HEPES, and 50 mM Tricine to determine pH dependence of the enzyme. Reactions were initiated by the addition of enzyme. The amount of NADPH oxidized was measured by monitoring the linear decrease in absorbance at 340 nm using a SHIMADZU UV-2450 UV-VIS spectrophotometer at 30 ºC. The mean data were obtained by at least three independent replicates. The initial velocity rates were calculated from the oxidation of NADPH, based on an absorption coefficient value of 6.22 mM^{-1} cm^{-1} for NADPH. The resulting rates were then divided by enzyme concentration to yield enzyme specific activity. Kinetic constants were calculated using SigmaPlot version 11.0.

Dependence of PAPR Activity/Inhibition Based on PAPS Concentration

The PAPR inhibition based on the substrate concentration was determined at two concentration of *E. coli* Trx of 10 μM and 1 mM. The assay condition was kept the same, as mentioned above, with the exception of the *E. coli* Trx concentration. The reaction rate was determined as a function of the substrate, PAPS. The Kinetic constants and inhibition constants were calculated using Graphpad 7.0. The inhibition was dependent on the concentration of the substrate, PAPS, and therefore fit the paradigm in which the second PAPS binds to the enzyme-substrate intermediate complex (E-Cys-S^{γ}-SO_3^{-}) as seen in equation 1b. Equation 1b was derived from the scheme seen in 1a [21].

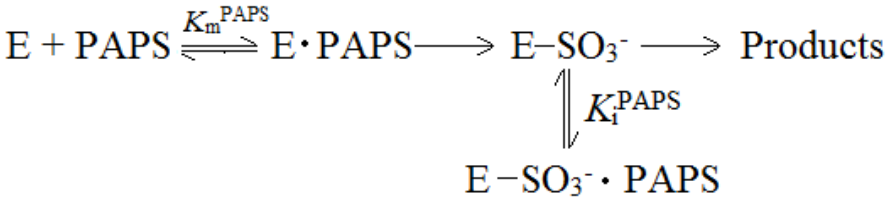

(1a)

$$v = V_{max}[PAPS] / K_m^{PAPS} + \{[PAPS](1 + [PAPS] / K_i^{PAPS})\} \quad (1b)$$

Ultraviolet-Visible Scanning of purified proteins

Samples of purified wild-type protein or the variants were analyzed spectrophotometrically between 200 nm and 600 nm, using a SHIMADZU UV-2450 UV-VIS spectrophotometer. The blank cell containing 30 mM Tris-HCl (pH 8.0) buffer with 100 mM Na_2SO_4 was used as the reference cell.

Mass Spectrometry

The purified proteins were incubated in 10 mM DTT at 37^0C for 15 minutes. The DTT-free proteins were collected via size-exclusion chromatography on a 10/300 GL Superdex column (GE Healthcare) equilibrated in 50 mM Tris 100 mM $NaSO_4$ (pH 8.0). The reduced proteins (WT, C19A, C22A, and C337A) were then incubated with 2-fold molar excess of PAPS for 10 minutes at 37^0C in order to create the Enzyme-thiosulfonate intermediate.

The mass spectrometry analysis used Accela liquid chromatograph tandem with LTQ Orbitrap Discovery mass spectrometer (Thermo Electron, Bremen, Germany) utilizing positive electrospray ionization (+ESI). In this method, the 5 µL of the sample was injected into a 15 cm x 2.1 mm extended C-18 column (Agilent Technologies, Palo Alto, CA) with the column temperature set at 30°C with a 400 µL/min flow rate. The

sample was eluted with a mobile phase (20-97%) consisting of acetonitrile and 0.1 % formic acid in water. A full-scan mass spectra (m/z range: 200 – 4000) of eluting compounds was obtained by orbitrap mass analyzer, which was then deconvulted by Xcalibur v.2.0.7 software. The following conditions were applied for a positive electrospray source: sheath and auxiliary gas flow 60 and 10 arbitrary units (a.u.), respectively; heated capillary temperature 275 °C; electrospray voltage 4.5 kV; capillary voltage 27 V; tube lens voltage 240 V.

Nonreducing SDS-PAGE

The Trx C35A variant from *E. coli* was expressed and purified as described above. The disulfide-linked Trx-MjPAPR adduct was formed by incubating the Trx C35A with MjPAPR (Wild-type, C19A, C22A, and C337A) with/without the substrate PAPS, at a 3:1 molar ratio of Trx:MjPAPR for 1.5 hours at room temperature. The samples were then loaded to a Non-reducing SDS-PAGE to identify which MjPAPR variant formed a disulfide-linked Trx-MjPAPR adduct.

Redox Potential of MjPAPR Wild Type and Mutants by mBBr Protein Titration

Purified MjPAPR protein (Wild-type, C19A, C22A, and C337A) were treated as followed, unless otherwise specified. The titration reaction was initiated with a freshly prepared 2 mM solution of oxidized DTT and reduced DTT (Sigma), which were prepared in 100 mM HEPES buffer pH 7.5. The oxidized and reduced forms of DTT were combined to a final volume of 1 ml in order to generate the different redox environments for the protein to be tested. A fixed amount of protein was added to each mixture and incubated for 3 hours at room temperature. Protein final concentration in solution is as follows: MjPAPR wild type: 1.01ng/µl; C19A: 1.06 ng/µl; C22A: 1.79

ng/µl; and C337A: 2.27 ng/µl. All protein concentrations were calculated with the Bradford method using a BSA standard curve. After the incubation, we added 7 µL of saturated monobromobimine (mBBr; Calbiochem) suspension in acetonitrile (Sigma; anhydrous 99.8%), which were mixed quickly and incubated in dark for 20 min. After incubation with mBBr, 500 µl of a 20% trichloroacetic acid (TCA 6,12M; BDH) was added to reach a 1:1 final ratio and incubate the mixture on ice for 30 minutes in the dark. Tubes were then centrifuged at 10 K for 15 minutes using a microfuge 16 from Beckman coulter and the supernatant was removed. Pellet was washed with 1% TCA, centrifuge at 10K for 5 minutes, and all the supernatant was carefully removed with a Pasteur pipette. Pellet was resuspended with 100 mM Tris-base pH 8.0 and 1% SDS in a final volume of 400 µl. Glass culture tubes containing 2.2 ml of 100 mM Tris-base pH 8.0 were used to dilute the resuspended protein and the fluorescent signal was recorded with a Shimadzu RF-5301PC spectrofluorophotometer with an Ex. 380 nm and Em. 425-450nm

CHAPTER THREE

Results

Sulfur assimilation has been thoroughly studied in both prokaryotes and eukaryotes [2, 10, 18, 19]. Both organisms utilize PAPS reductase or APS reductase to produce sulfite, which will eventually be reduced into a usable sulfur source [2, 10, 18, 19]. In particular, PAPS reductase exists mostly in the sulfate assimilation pathway [18, 19]. Although sulfate assimilation has been explored for prokaryotes and eukaryotes, little to none is known about sulfate assimilation mechanism in archaea. Due to the possible presence of PAPS reductase in the archaeon *Methanocaldococcus jannaschii* [3], we investigated the identity of PAPS reductase.

ORF Mj0066 Encodes *Methanocaldococcus jannaschii* PAPS reductase

Mj0066 was annotated as a sulfur trasferylase enzyme [3]. To study the gene *Mj0066*, we cloned, expressed, purified, and checked it for PAPS reductase activity. We expressed the recombinant gene *Mj0066*, which appended a six-histidine tag at the N-terminus to facilitate the purification of the enzyme from the *E. coli* host. The purity of the protein was checked with SDS-PAGE analysis (Figure. 2), which indicated that the wild-type Mj0066 showed a single major Coomassie-staining band (>95% purity) corresponding to a molecular mass of ~60 kDa. The exact mass of Mj0066 was confirmed as 60,495.0 Da by ESI-orbitrap mass spectrometry, which is in agreement with the calculated mass of 60495.9 Da (Figure 7).

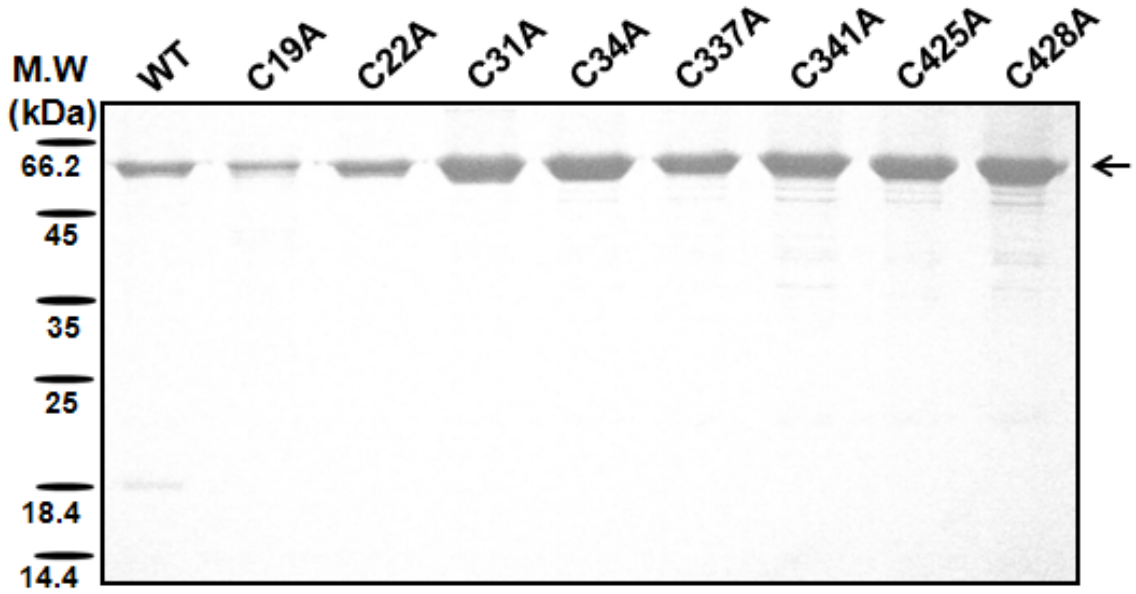

Figure 4. SDS-PAGE of purified recombinant wild- type and mutant proteins. Molecular size markers (M.W). The gel was stained with Coomassie Brillant Blue R250.

The *Mj0066* sequence was aligned with prokaryote and eukaryote, *E. coli* PAPS reductase (EcPAPR) and *S. cerevisiae* PAPS reductase (ScPAPR), respectively, as seen in Figure 5. According to the sequence alignment, archaea Mj0066 shared several key motifs and numerous conserved residues with EcPAPR and ScPAPR. Although the C-terminus cysteine was not conserved, all three (EcPAPR, ScPAPR, and Mj0066) contained the conserved pyrophosphate-binding motif, DT motif, and an arginine loop, which make up the binding site of the PAPS reductase [2, 6, 10, 20, 21]. Thus, the sequence alignment of Mj0066 with EcPAPR and ScPAPR suggested that Mj0066 could potentially be a novel PAPS reductase.

The PAPS reductase activity was measured by enzyme assay, using various concentrations of substrates (either APS or PAPS) and with saturating concentrations of electron donors (either glutaredoxin or thioredoxin). It was determined that Mj0066 has

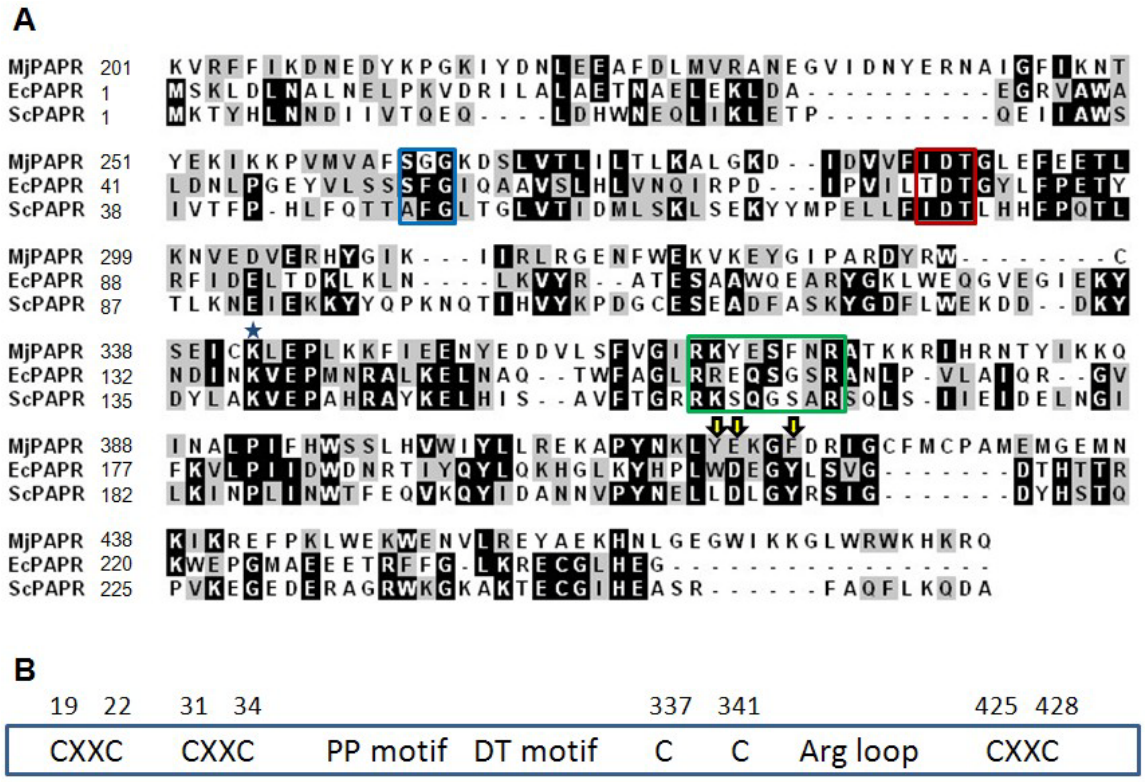

Figure 5. Amino acid sequence alignment and a domain diagram of Mj0066. Sequences were obtained from the NCBI sequence databases. Alignment was performed by ClustalW with BioEdit. A. Sequence alignment of putative PAPR region in Mj0066 with *Escherichia coli* PAPR (EcPAPR) and *Saccharomyces cerevisiae* PAPR (ScPAPR). The blue box represents the PP-motif. The red box represents the DT-motif. The green box represents the arginine-loop. The three arrows represents the Trx stacking region. B. The diagram presents putative PAPR region in Mj0066 (amino acid region of 257-424) and the Cys residues used for site-directed mutagenesis.

substrate specificity for PAPS with the K_m *and* V_{max} value of 15.9 μM and 0.09429 μmol/mg/min, respectfully, using Trx as the electron donor (Table 2). From this, we calculated a k_{cat} of 0.08859s^{-1} and a catalytic efficiency (k_{cat}/K_m) of 5571$M^{-1}s^{-1}$. In addition to kinetic analysis, Mj0066 was scanned under UV-Vis for possible cofactors. The cofactor analysis revealed that Mj0066 lacks cofactors, such as iron-sulfur clusters (Figure. 4). The absence of any cofactors is a common characteristic of a PAPS reductase [22,23]. These data propose that the protein expressed by *Mj0066* is a PAPS reductase and will now be referred to as MjPAPR.

Table 2. Kinetic Parameters of MjPAPR

Substrate	Electron donor	K_m(μM)	V_{max}(μmol/mg·min)	k_{cat}(1/s)	k_{cat}/K_m(1/M·s)
APS	Trx	None*	None	None	None
APS	Grx	None	None	None	None
PAPS	Trx	15.9	0.09429	0.08859	5571
PAPS	Grx	None	None	None	None

1mM Recombinat Trx or Grx from *E.coli* was used as electron donor. *None indicates there was no detectable activity.

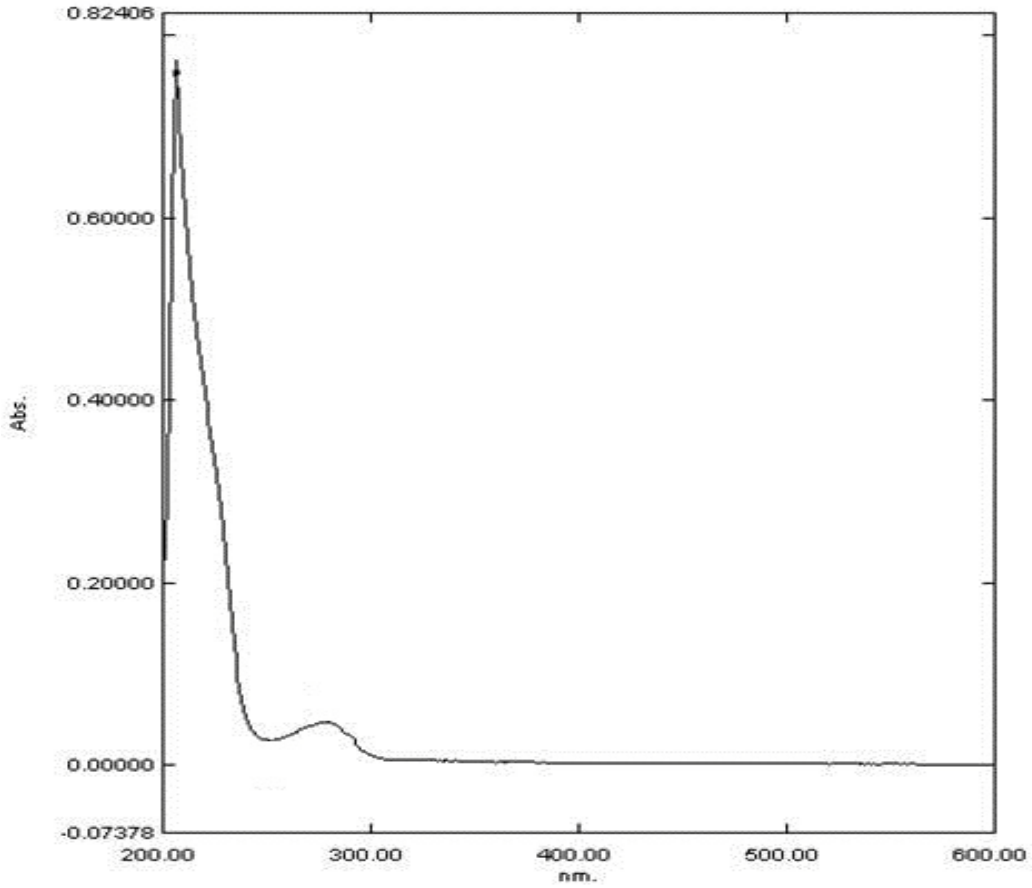

Figure 6. Cofactor analysis of MjPAPR from 280 nm to 600 nm. There is no sign of any cofactors in this spectrum.

Role of Cysteine Residue in the Catalytic Mechanism

Previous studies with sulfonucleotide reductase from various organisms had displayed the importance of the C-terminal cysteine residue in the catalytic activity [2, 10, 19, 20]. However, MjPAPR lacks the C-terminal cysteine while possessing PAPS reductase activity. In order to investigate the role of cysteine in the catalytic mechanism, site-directed mutagenesis was carried out to obtain the location of the catalytic cysteine. We successfully mutated, expressed, and purified eight single cysteine variants (C22A, C31A, C34A, C337A, C341A, C425A, and C428A) for every individual cysteine in MjPAPR (Figure. 3B) using specific oligonucleotide primers for site-directed mutagenesis (Table 1). The purified mutants showed a single major Coomassie-staining band by SDS-PAGE analysis, which indicated >95% purity (Figure. 2). The mutants underwent the enzyme assay in order to determine PAPS reductase activity. The results showed that variants C19A, C22A, and C337A had very little to no PAPS reductase activity (Table 3), which suggests Cysteines at 19, 22, and 337 appear to be involved in the catalytic mechanism.

To test whether cysteine 19, 22, or 337 were essential for the formation of enzyme-sulfonucleotide intermediate, the three variants (C19A, C22A, and C337A) were incubated with the substrate (PAPS) and sprayed directly for mass spectrometry analysis. The mass analysis showed a shift in mass of +80 Da in Wild-type, C19A and C22A variants (Figure 5, Figure 6, and Figure 7), but none in C337A variant (Figure 8), suggesting that only cysteine 337 is involved in the nucleophilic attack of the substrate. Theoretically, +80 Da shift corresponds to the sulfite (with molecular weight of 80 Da) binding to the enzyme.

Table 3. PAPS Activation of Wild Type and Variants of MjPAPR

Enzyme	K_m(μM)	V_{max}(μmol/mg·min)	k_{cat}(1/s)	k_{cat}/K_m(1/M·s)
W.T	15.9	0.09429	0.08859	5571
C19A	None*	None	None	None
C22A	None	None	None	None
C31A	15.9	0.07059	0.06632	4171
C34A	19.8	0.06882	0.06466	3266
C337A	None	None	None	None
C341A	16.2	0.06471	0.06080	3753
C425A	31.2	0.07551	0.07094	2274
C428A	4.6	0.03300	0.03100	6740

1mM Recombinat Trx from *E.coli* was used as electron donor. *None indicates there was no detectable activity.

Prior sulfonucleotide reduction studies have shown that the catalytic cysteine found on the C-terminal nucleophilically attacks the substrate and forms an enzyme-sulfonucleotide intermediate until the electron donor releases the product [10]. Therefore, the lack of mass shifts in C337A variant with the substrate (PAPS) advocates that Cys337 is responsible for the catalytic attack on the substrate and analogous to the C-terminus cysteine.

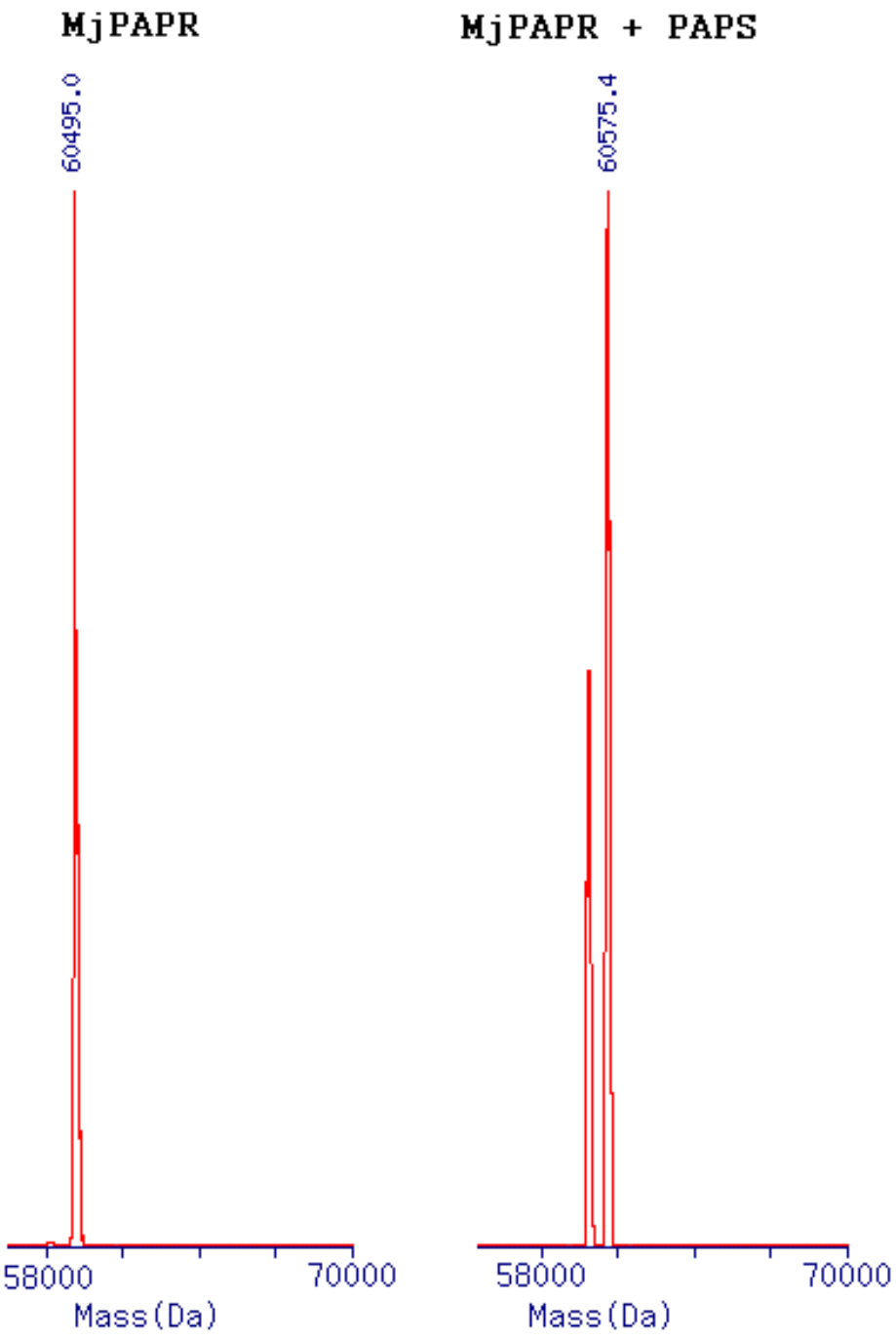

Figure 7. Deconvoluted mass spectrum of MjPAPR without substrate and MjPAPR with substrate PAPS bound.

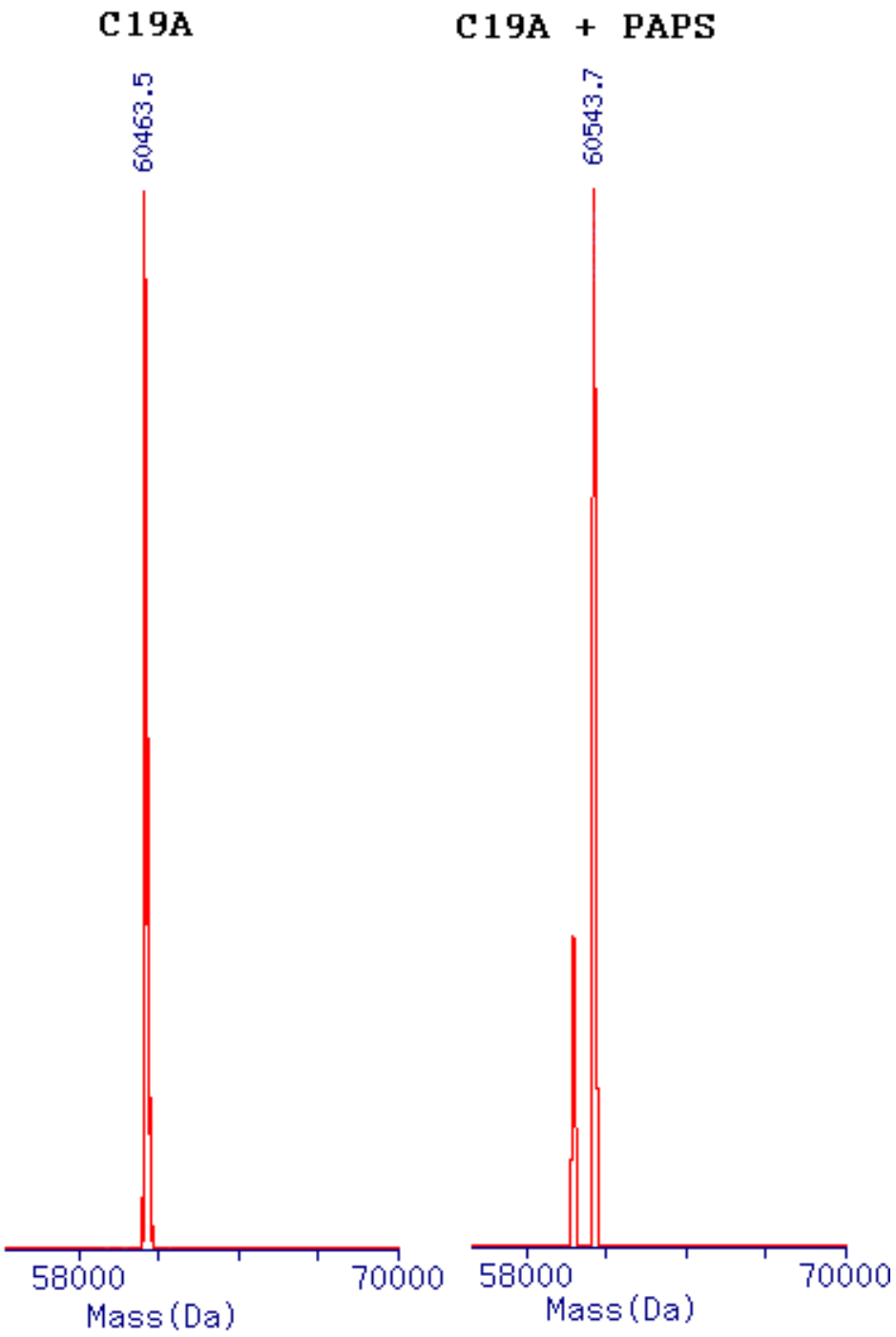

Figure 8. Deconvoluted mass spectrum of MjPAPR variant C19A without substrate attached and with substrate PAPS bound.

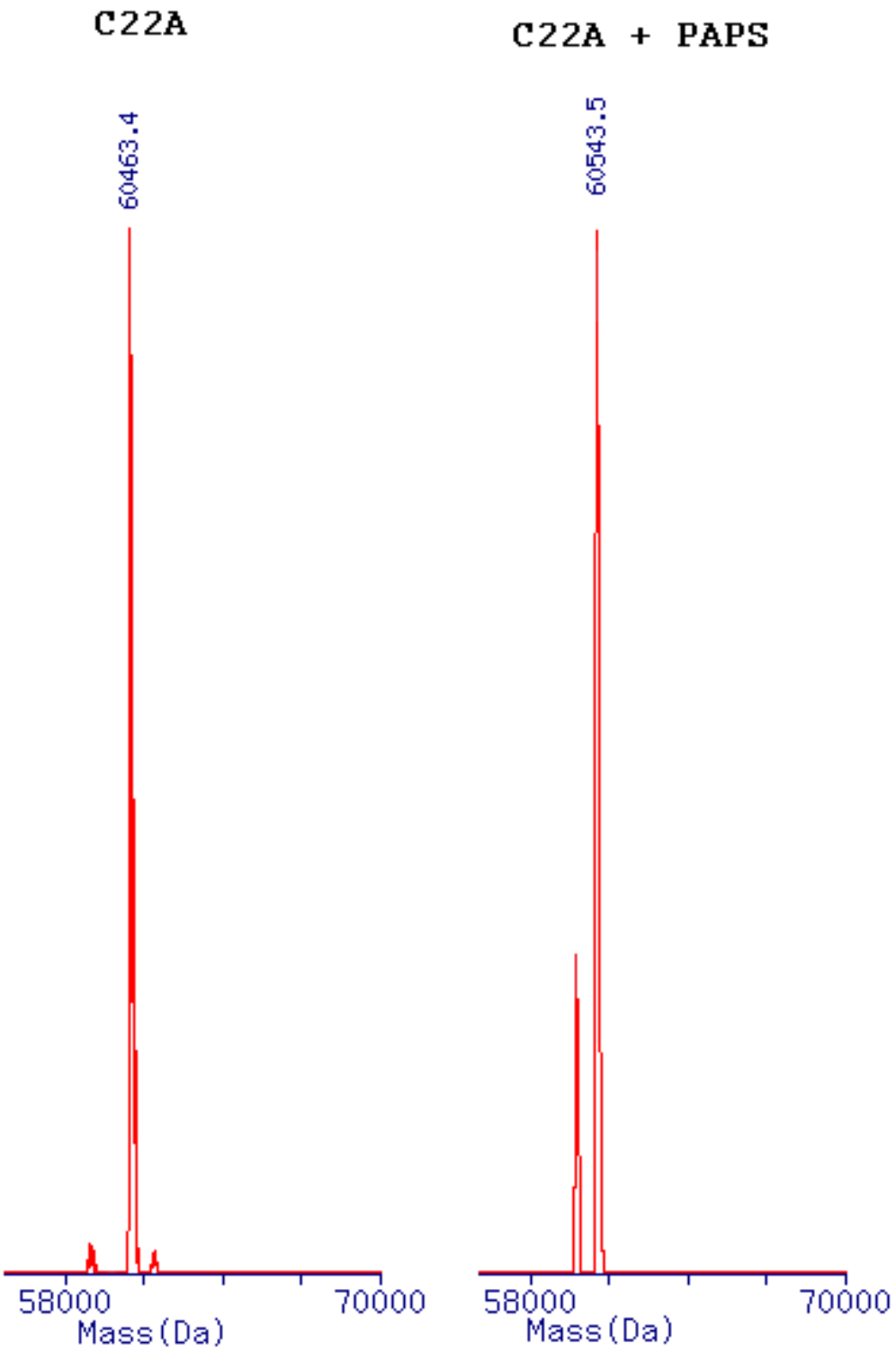

Figure 9. Deconvoluted mass spectrum of MjPAPR variant C22A without substrate attached and with substrate PAPS bound.

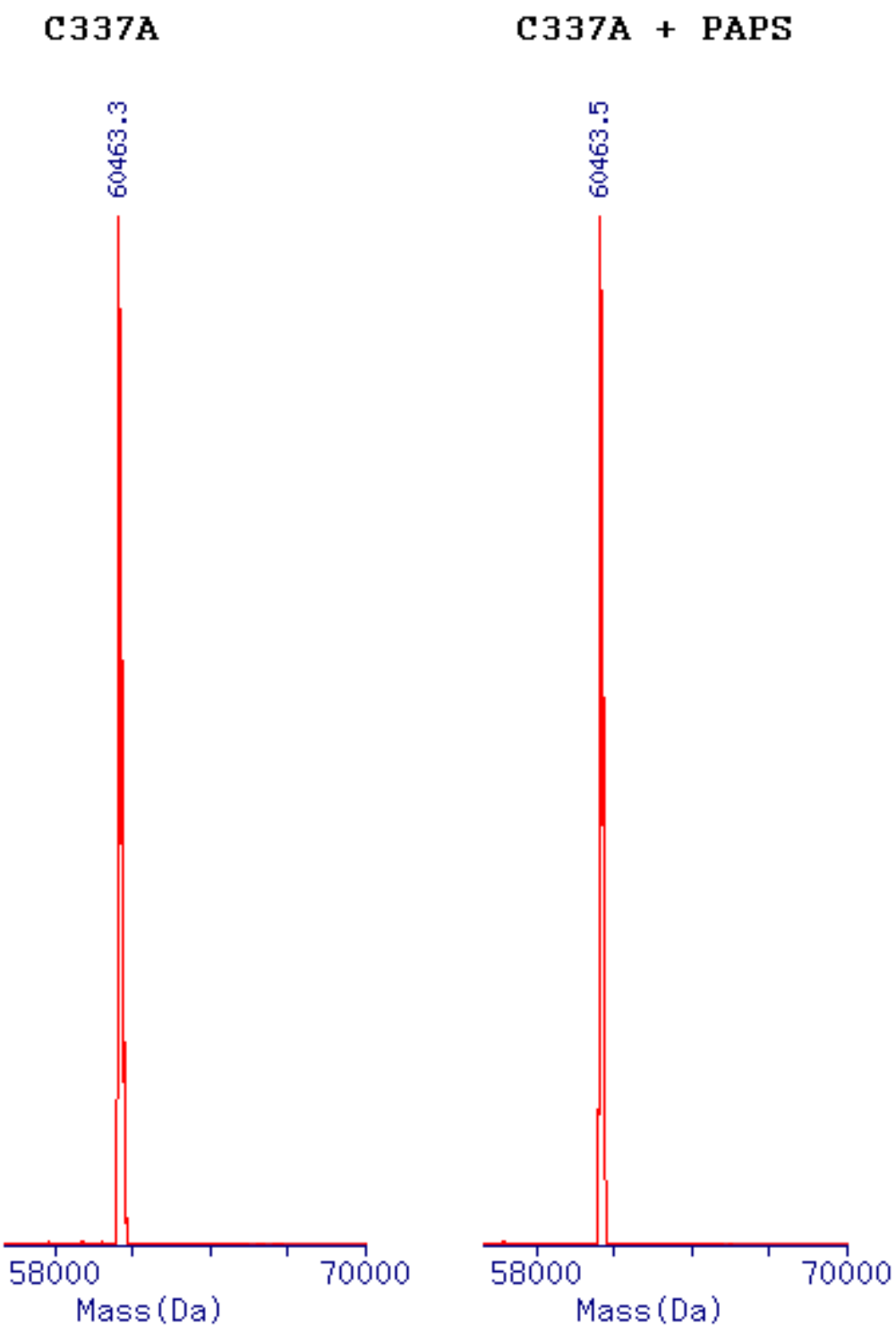

Figure 10. Deconvoluted mass spectrum of MjPAPR variant C337A without substrate attached

Role of Trx in the Catalytic Mechanism

Prior works have demonstrated that upon formation of the enzyme-sulfonucleotide intermediate, the electron donor (Trx) cleaves the thiol bond between the enzyme and the substrate and release the product, sulfite [2, 10, 19]. The conserved sulfonucelotide reduction mechanism states that the intermediate will be formed in the absence of Trx, and the addition of Trx will lead to the production of the product and regeneration of the enzyme [19]. Cys35 was mutated to alanine (Trx C35A) so that we may observe two distinct interactions between the enzyme intermediate and Trx. (1) The formation of enzyme-sulfonucleotide intermediate in the absence of Trx, and (2) product release in the presence of Trx.

We can see the formation of the enzyme-sulfonucleotide intermediate in the absence of Trx (Figure 5). Before we saturated the enzyme (MjPAPR) with an excess of the substrate (PAPS), its molecular weight was 60,495.0 Da. We saw a shift in mass to 60,575.4 Da (+80 Da) when MjPAPR was incubated with PAPS, indicating the successful formation of the intermediate. Also, previous studies have shown that when the concentration of Trx is limiting, the elevating concentrations of the substrate (PAPS) will result in substrate inhibition in sulfonucleotide reduction [10, 21]. Figure 11 shows that inhibitory effect in MjPAPR is evident once the concentration of PAPS is above its K_m of 15.9 μmol, and PAPS acts as a competitive inhibitor. The K_i increases from 31.78 μM to 76.21 μM upon increasing the concentration of Trx from 10 μM to 1 mM, respectively. Furthermore, the kinetic data (Figure 10) indicate that the MjPAPR activity is dependent on two substrates (PAPS and Trx), and possibly possesses a ping-pong mechanism (Figure 11) as seen in EcPAPR [24]. These data were in agreement with the

first step in the conserved sulfonucleotide mechanism that states the formation of the enzyme-sulfonucleotide intermediate is independent of Trx [19].

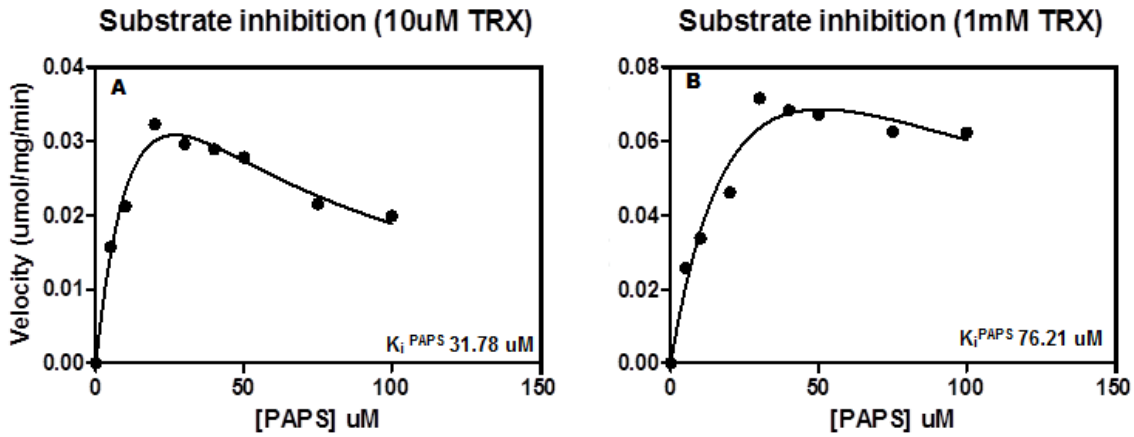

Figure 11. A. Substrate inhibition curve showing the substrate (PAPS) will act as an inhibitor to the enzyme with 10 μM of Trx. The K_m and K_i is 12.99 μM and 31.78 μM, respectively. B. Substrate inhibition curve showing the substrate (PAPS) will act as an inhibitor to the enzyme with 1 mM of Trx. The K_m and K_i is 15.91 μM and 76.21 μM, respectively.

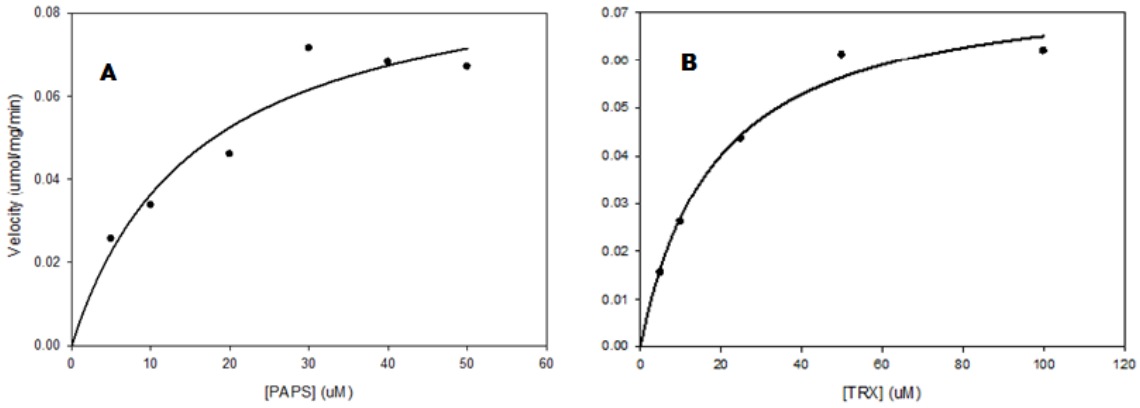

Figure 12. A. Michaelis-Menton curve of MjPAPR using PAPS as substrate. Fixed concentration of 1 mM recombinant *E. coli* Trx is used as an electron donor. K_m for MjPAPR utilizing PAPS as a substrate is 15.9 μM with V_{max} of 0.0942 μmol/mg/min. B. Michaelis-Menton curve of MjPAPR using *E. coli* Trx as a substrate. Fixed concentration of 30 μM PAPS is used for the reaction. K_m for MjPAPR utilizing Trx as a substrate is 18.4 μM with V_{max} of 0.0771 μmol/mg/min.

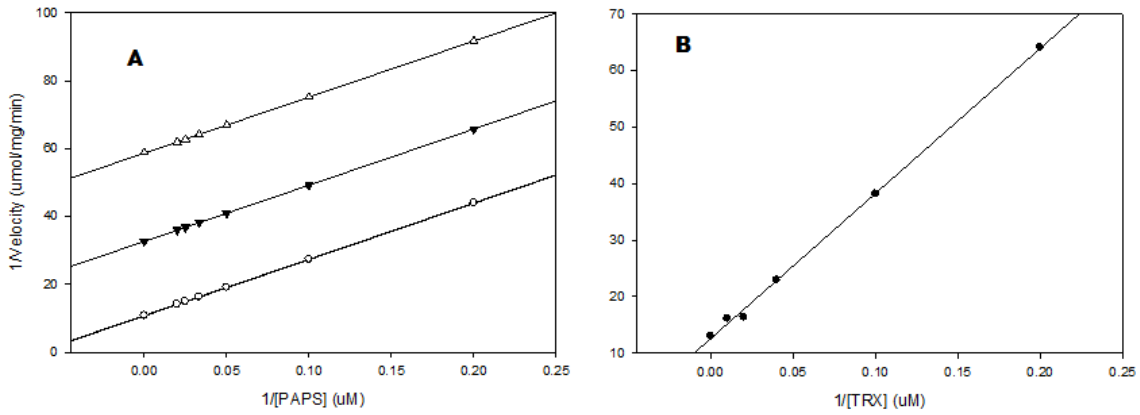

Figure 13. A. Reciprocal plot analysis of MjPAPR. The concentration of PAPS varies at different fixed concentrations of E. coli Trx(●)(50 uM, (▼) 10 uM, and (Δ) 5 uM. B. Lineweaver Burke plot of MjPAPR using *E. coli* Trx as a substrate.

The second observation was uncanny compared to the expected outcome. We expected to see the formation of the Trx-Enzyme adduct only in the presence of enzyme-sulfonucleotide intermediate. If the enzyme was not incubated with PAPS prior to saturation with Trx C35A, adduct should not form. However, the formation of the adduct occurred regardless of PAPS (Figure 14). Another interesting observation was absence of the adduct formation in the MjPAPR variant C19A, which suggests that the Cys37 of Trx will attack and bind at the Cys19 of MjPAPR. This idea was supported by the result of redox titration of MjPAPR and its variants with mBBr (Figure 15, 16, 17, and 18). The MjPAPR wildtype and its variant C337A maintains potential (Figure 15 & 16), which advocates that cysteine 337 is not involved the redox mechanism of MjPAPR. However, C22A has very miniscule level of potential while C19A has virtually none (Figure 17 & 18). The absence of potential in C19A variant proposes that cysteine 19 is involved in the electron transfer between the MjPAPR and its electron donor Trx. Additionally, the relatively low potential seen in C22A variant can be attributed cysteine 22's indirect role in the electron transfer mechanism. Taking into account what we saw,

we postulate that formation of the Trx-enzyme adduct is independent of the formation of enzyme-sulfonucleotide intermediate, which is contrary to the conserved mechanism, and that the redox site for Trx is at cysteine 19 of MjPAPR.

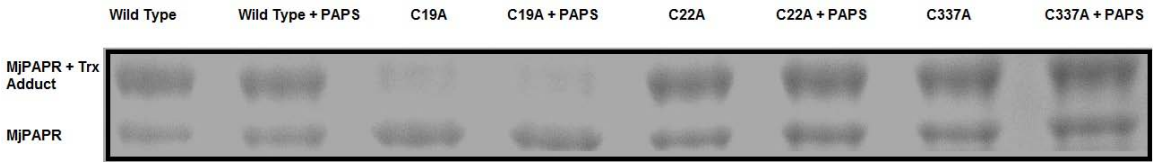

Figure 14. Non-reducing SDS-PAGE. The gel shows that C19A variant cannot form an adduct with the *E. coli* Trx C35A, while successfully forming an adduct with MjPAPR wild-type, C22A, and C337A.

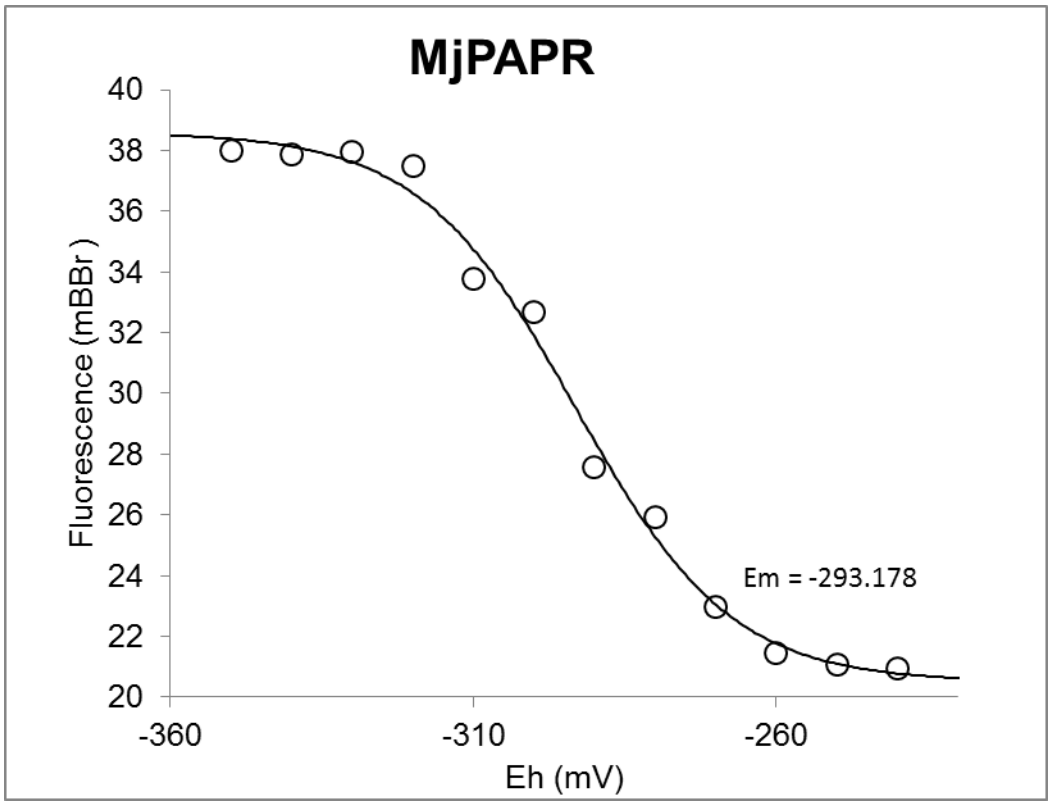

Figure 15. Titration curve of MjPAPR wildtype with mBBR.

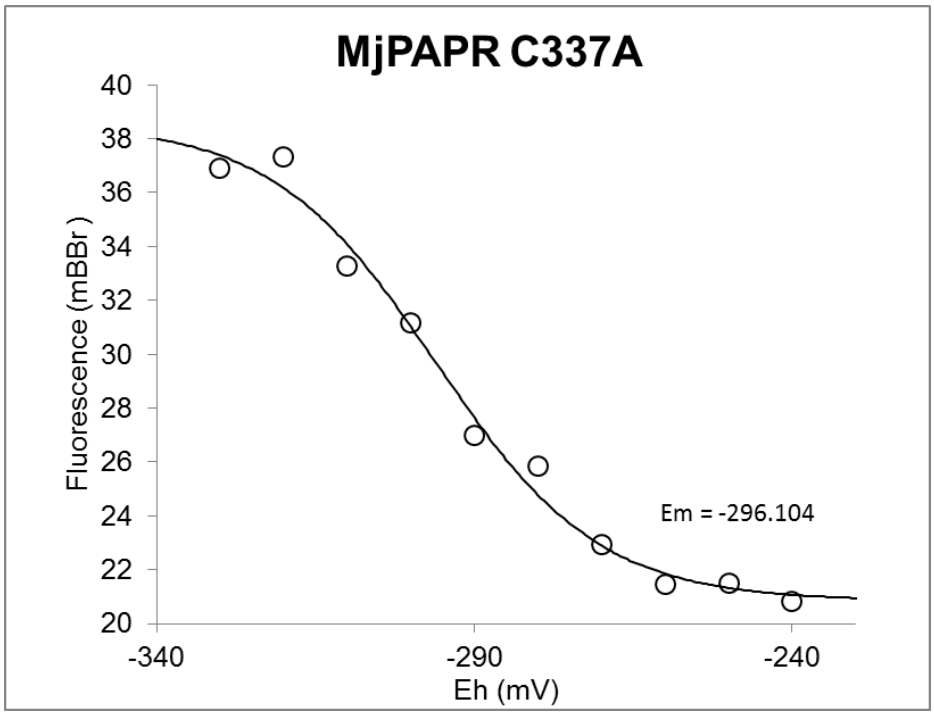

Figure 16. Titration curve of MjPAPR variant C337A with mBBR.

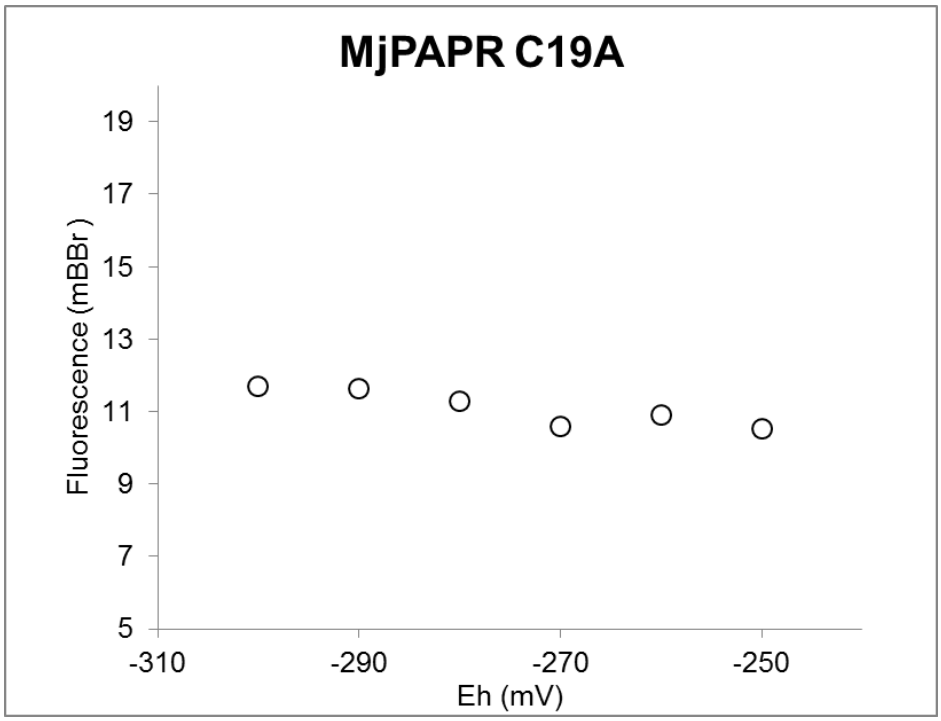

Figure 17. Titration curve of MjPAPR variant C19A with mBBR.

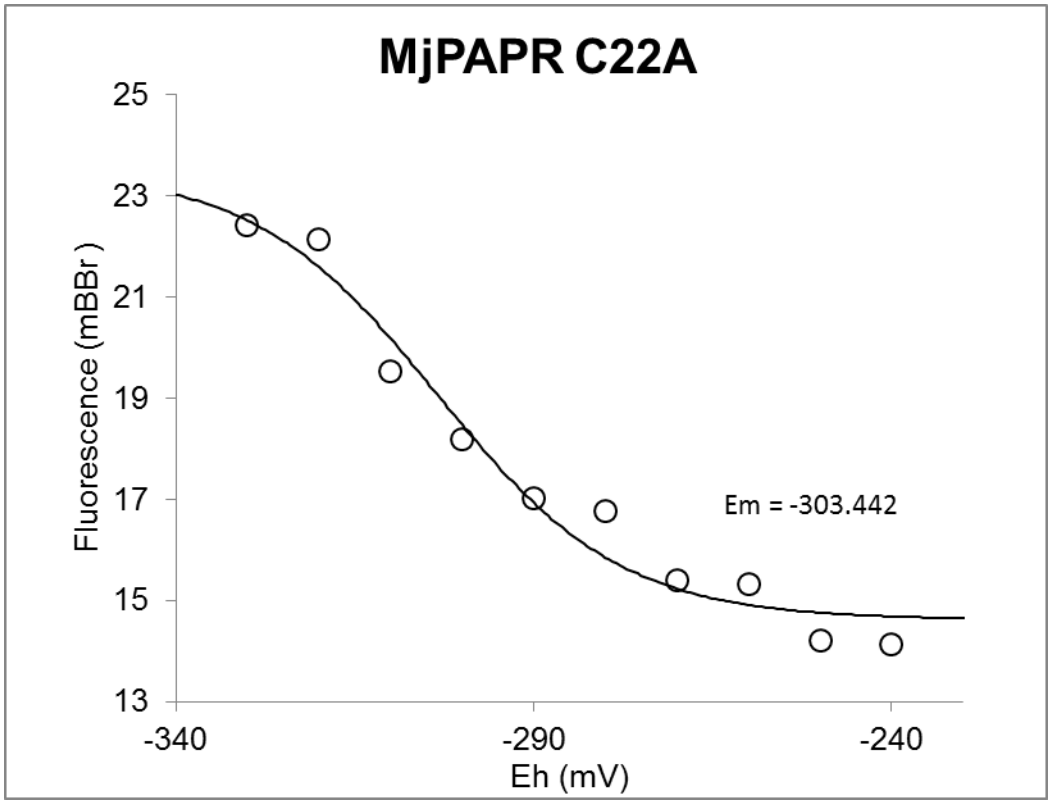

Figure 18. Titration curve of MjPAPR variant C22A with mBBR.

CHAPTER FOUR

Discussion

Determination of PAPS reductase in M. jannaschii

Our results provide the first convincing evidence that *M. jannaschii* reduces PAPS using a previously hypothetical archaeal enzyme. In our amino acid sequence alignment, the putative PAPS reductase region of *Mj0066* (amino acids 257 to 424) shares structurally and catalytically important conserved regions with PAPS reductase from *Escherichia coli* (EcPAPR) and *Saccharomyces cerevisiae* (ScPAPR), thus suggesting the possible presence of PAPS reductase in *M. jannaschii*. Confirming the amino acid sequence alignment, our kinetic study revealed that the MjPAPR indeed possesses PAPS reductase activity. The kinetic study also indicated that the activity of MjPAPR is dependent on Trx like other PAPS reductase. Therefore, we have revealed that the protein produced by the gene *Mj0066* acts as a PAPS reductase mediated by Trx.

Active Site of PAPS Reductase in M. jannaschii

The data acquired from the amino acid sequence alignment show that MjPAPR is expected to possess an active site similar to other PAPS reductases. Previous amino acid sequence alignment of PAPS reductase from different organisms identified key conserved motifs, such as the PP motif, DT motif, and an arginine-rich sequence [2, 6, 10, 21, 23]. It has been speculated that these key conserved motifs are involved in the construction of the active site in PAPS reductase [2, 6, 10]. Specifically, the crystal structures of EcPAPR-Trx complex and ScPAPR-3'-phosphoadenosine 5'-phosphate (PAP) complex established the role of the motifs as substrate binding factors of the active site (Figure 17,

Figure 18) [2, 10]. Since our sequence alignment analysis reveals that the MjPAPR shares these important conserved motifs with EcPAPR and ScPAPR, the active site of MjPAPR is presumably constructed in a similar fashion.

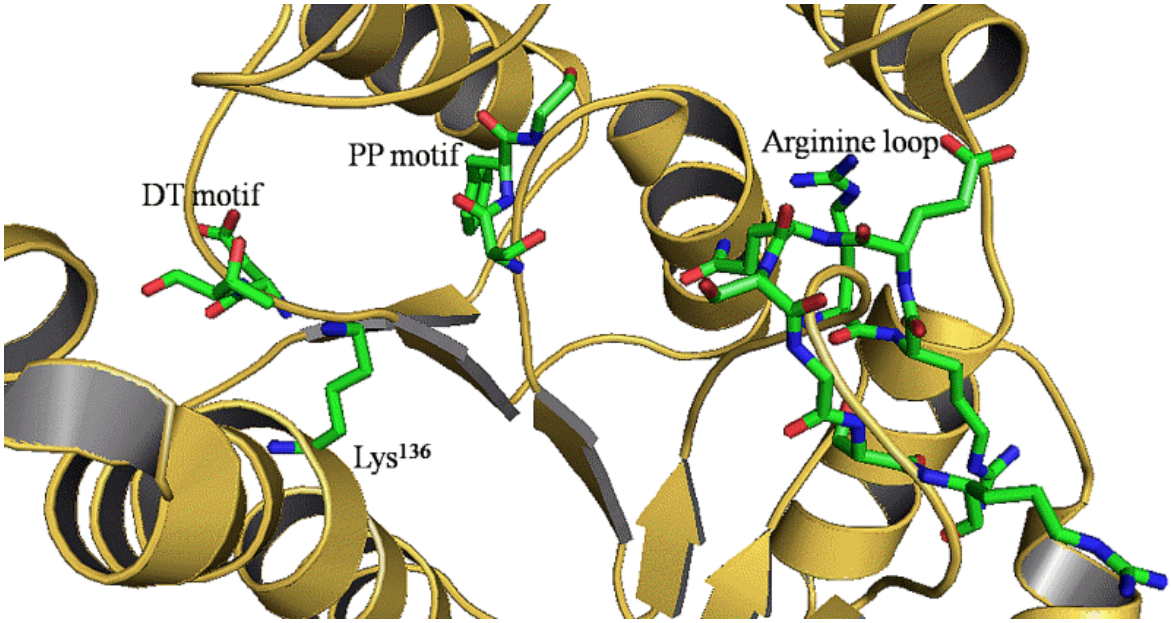

Figure 19. Active site of EcPAPR. The 3-D structure of EcPAPR was obtained from Protein Data Bank (PDB entry: 2O8V). Stereoview of the EcPAPR active site is shown with the residues of highly conserved motifs, including the PP-motif (^{53}SFG^{55}), Arg loop (^{157}RREQSGR^{164}), DT motif (^{77}DT^{78}) and the sulfate binding Lysine residue (K^{136}), present by stick models.

From our amino acid sequence alignment, we observed that MjPAPR possesses the conserved PP motif (263SGGKDS268). The PP motif, which is conserved in sulfornucleotide reductases, was originally proposed to interact the 5'-phosphosulfate moiety of APS/PAPS [20]. However, according to crystal structure studies of EcPAPR and ScPAPR (Figure 17 and Figure 18), the first serine of the PP motif is actually placed in a position that forms hydrogen bond with the 3'-phosphate of the PAPS [2, 6]. Moreover, the 3'-phosphate oxygen of the PAPS could potentially hydrogen bond with

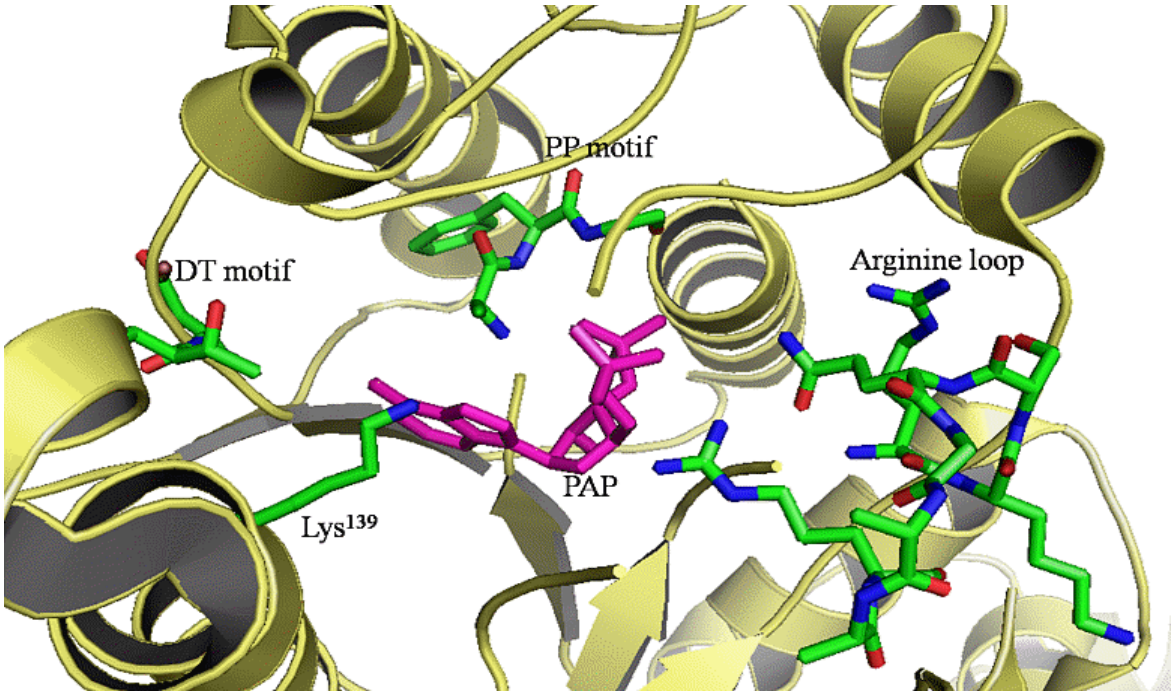

Figure 20. Active site of ScPAPR. The 3-D structure of ScPAPR was obtained from Protein Data Bank (PDB entry: 2OQ2A). Stereoview of ScPAPR bound to its product PAP in the active site is shown with the same highly conserved motifs, PP-motif (49AFG51), Arg loop (161KSQGSARSQLS171), DT motif (77DT78), and the sulfate binding Lysine residue (K139). The product PAP (colored in magenta) and conserved motifs are displayed in stick model.

the main chain amide nitrogen of the serine and the glycine of the PP motif found in the anion-binding site of the enzymes [2, 6]. Therefore, the PP motif in MjPAPR seemingly serves as the potential binding site for 3'-phosphate of PAPS, as seen in other PAPS reductase.

The amino acid sequence alignment also shows that MjPAPR is expected to possess multiple PAPS purine ring-binding sites, located at Ile^{288} of the DT motif and/or Lys^{342}. According to the crystal structure study of the ScPAPR-PAP complex, the isoleucine of the DT motif (^{76}IDT^{78}) was determined to a purine binding site [2]. Ile76 of ScPAPR forms a hydrogen bond with the N1 and N6 of the adenine ring [2]. Thus,

because Ile^{76} of ScPAPR is aligned with Ile^{288} of MjAPR in the sequence alignment, hydrogen bonding interactions between the adenine ring of PAPS and the DT motif of MjPAPR, specifically Ile^{288}, are expected. In addition, the crystal structure study of EcPAPR suggests that the highly conserved Lys^{136}, which is homologous to Lys^{342} of MjPAPR, points into the substrate-binding site towards to the purine ring of PAPS [6], possibly indicating the presence of another purine ring binding site in the MjPAPR.

Notably, the highly conserved lysine has been shown to adopt multiple conformations, and in turn, multiple functions [30]. Recent crystal structure studies of APRs and PAPRs suggest that this conserved lysine binds with the sulfate moiety of the substrate [2, 10, 21]. In *Pseudomonas aeruginosa* APS Reductase (PaAPR), EcPAPR, and ScPAPR, the conserved lysine (Lys144 of PaAPR, Lys 136 of EcPAPR, and Lys139 of ScPAPR) appears to interact with the sulfate moiety of the substrate [2, 10, 21]. Hence, Lys342 in MjPAPR is both considered as a possible purine ring binding site and a possible PAPS sulfate moiety binding site.

Our results evince that MjPAPR contains an additional key conserved region found within PAPRs: the arginine loop (the sequence starting from Arg365 to Arg372). The importance of arginine residues in the loop is their ability to form multiple interactions with the substrate and their frequent utilization as ligands for binding anions to the protein [25]. In the case of phosphoglycerate kinase, which is another arginine-loop possessing enzyme found in pig muscle, the arginine residues are observed to function similarly by binding to the substrate phosphate group [26]. More specifically, the crystal structure study of ScPAPR showed that the Arg167 and Arg 236, which is homologous to Arg365 and Arg372 of MjPAPR, respectively, binds the 5'-phosphate of

the PAP [2]. Therefore, the arginine loop in MjPAPR could be considered as a viable 5'-phosphate binding site.

Our study also shows that MjPAPR possesses a potential aromatic stacking region (comprised of Tyr404, Tyr412, Tyr416, Glu417, and Phe420) that stabilizes the PAPR with the electron donor, Trx. A recent crystal structure study of EcPAPR in complex with Trx suggested that the aromatic stacking residues Tyr191, Tyr201, Trp205, Asp206 and Tyr209 are involved in the interaction that assists the binding between the PAPR and the Trx [6, 10]. The Tyr191 is involved in aromatic stacking interaction with the Trp31 of Trx [6]. Tyr201 is associated in the aromatic stacking interaction with Trp205, thereby positioning Trp205 in a favorable conformation to interact with the Trx [6]. Furthermore, Trp205 was determined to hydrogen bond with the carbonyl of Glu30 of Trx, thus stabilizing the EcPAPR-Trx complex [10]. Asp206 interacts with the Lys36-Glu30 salt bridge of the Trx [6]. Tyr209 is responsible for stabilizing the surface interaction between the enzyme and Trx [6]. Our sequence alignment has shown that the Tyr191 and Tyr201 in EcPAPR are conserved as Tyr404 and Tyr412 in MjPAPR, respectively. However, Trp205, Asp206 and Tyr209 in EcPAPR have been altered to Tyr416, Glu417, and Phe420, respectively. Although there is transformation in the latter three aromatic stacking residues, the functional groups between the homologous modified residues are strikingly similar. Hence, the conserved and slightly variant aromatic stacking residues in MjPAPR are likely to assemble the potential aromatic stacking region responsible for stabilizing the enzyme-Trx complex.

A Distinct Enzyme-Thiosulfonate Intermediate and A Novel CXXC redox motif

The universal sulfonucleotide reduction mechanism strongly emphasizes on the formation of the enzyme-thiosulfonate intermediate (E-Cys-S-SO_3^-) [19]. APS reductase and PAPS reductase from various organisms all form this intermediate by forming a thiol bond between the catalytic cysteine found in the ECG(I/H)L motif and the sulfate-moiety of the substrate [2, 10, 19, 21, 22]. Our results are not completely consistent with the statement above since MjPAPR lacks the highly conserved ECG(I/L)H motif. However, our mutational analysis provided evidence that supports the potential existence of an alternative catalytic cysteine in MjPAPR (Cys337), which showed no activity and was unable to form a covalent intermediate with the sulfate of PAPS when it was mutated into alanine. In addition, Cys337 is in proximity to the highly conserved residue Lys342, which could be the sulfate moiety binding site in the substrate-binding pocket of PAPS Rreductase [2, 6, 10, 19, 21]. Accordingly, our mutational analysis and the close proximity of Cys337 to Lys342 suggest that the Cys337 possibly functions as a catalytic residue in the active site of MjPAPR that will form the distinct enzyme-thiosulfonate intermediate.

Furthermore, the conserved sulfonucleotide reduction states that an electron donor is required to cleave the thiosulfonate in order to release the product, sulfite [9, 19, 21]. The electron donor is able has access to the thiosulfonate intermediate because the ECG(I/L)H motif is located on the C-terminus tail, which is displaced out of the binding site upon substrate binding [19, 21]. However, the location of the catalytic cysteine (Cys337) of MjPAPR does not allow the enzyme-thiosulfonate intermediate to be accessible to the electron donor. Our data postulate that there can be a feasible, novel

redox motif on the N-terminal tail that allows the transfer of the two electrons required for the reduction of sulfite.

Based on the mutational analysis of the two potential redox active cysteine residues (^{19}CXXC^{22}) located on the N-terminal tail, we propose that these N-terminal cysteines are prospective Trx-like reducing cysteines. Upon mutagenesis of either one of these cysteines, there was no trace of activity in the MjPAPR, suggesting its possible redox reaction with the electron donor, Trx. Typically, the active site of Trx contains two cysteine residues, which function as a redox-active disulfide/dithiol linked-bridge [27]. The first step of the Trx mechanism begins with the active-site cysteine of Trx attacking the disulfide bond of an oxidized target substrate [27, 28]. This, in turn, forms a transient disulfide bond between the Trx cysteine and the cysteine on the target substrate [27, 28]. Following the formation of the disulfide bond between the Trx and the substrate, the second Trx cysteine carries out a nucleophilic attack on the intermolecular disulfide, producing oxidized Trx and the reduced thiol cysteines while transferring two electrons [27, 28]. The Trx-driven mechanism appears to follow the ping-pong mechanism since the enzyme transfers two electrons from the reduced Trx to an oxidized substrate [29]. The resulting electrons obtained from the Trx are stored in the enzyme, which upon reduction converts the enzyme into a stable reduced state [30]. In the case of PAPR in *Bacillus subtilis* (BsPAPR), the transfer of two electrons to BsPAPR converts the enzyme into a stable reduced state, which then reacts with the PAPS, displacing the sulfite and the PAP [23]. Comparably, the disulfide bridge of the oxidized ^{19}CXXC^{22} residues of MjPAPR is seemingly involved in redox reaction with the reduced Trx. After the redox active cysteines are reduced by the Trx, the two cysteines potentially possess the ability

to transfer two electrons and reduce another disulfide bridge, such as the thio-sulfonate intermediate, thus establishing a stable reduced enzyme state. Therefore, the Trx-dependent reduction mechanism in MjPAPR seems to utilize ^{19}CXXC^{22} as the relay center to transfer two electrons from the Trx to the enzyme. In addition, the non-reducing gel showed that Trx C35A variant will not form an enzyme-Trx adduct without the presence of Cys19, which is allegedly where the dithiol linked-bridge will occur between the Trx and MjPAPR. This novel redox site on the N-terminal tail seems plausible due to the inaccessible location of the enzyme-thiosulfonate intermediate. Because MjPAPR's catalytic cysteine in not located on the flexible tail on the C-terminal, it seem possible that the N-terminal tail could possess the means to store two electrons from Trx and fold to donate the electrons to the rigid enzyme-thiosulfonate intermediate.

Sulfonucleotide Reduction Mechanism for MjPAPR

Our mutational analysis reveals that individual Cys/Ala variants C19A, C22A, and C337A lack activity, highlighting the importance of Cys19, Cys22, and Cys337 residues in the PAPS-dependent sulfate reduction mechanism. Two important factors have been suggested in the conserved mechanism for sulfonucleotide reduction. First, a catalytic cysteine attacks the β-sulfate of the PAPS substrate, and secondly, the sulfite is released in a Trx-dependent reaction [2, 10, 19, 30]. Previous crystal structure studies of EcPAPR and ScPAPR have established that Cys239 of EcPAPR and Cys245 of ScPAPR are catalytic cysteines involved in the reduction mechanism since they are in the highly conserved ECG(I/L)H motif located on the C-terminal tail [2, 10]. Upon the substrate binding in the active site, the PAPR undergoes a conformational change that moves the C-terminal tail directly over the active site [10]. The catalytic cysteine then attacks the

sulfate of the substrate, thereby, creating an Enzyme-S-sulfocysteine intermediate plus PAP [10]. Finally, the intermediate is ready to interact with the Trx, which will reduce the intermediate and displace the reduced sulfite [10].

As stated before, MjPAPR is unique in comparison to most sulfonucleotide reductases in two aspects: the unconventional catalytic cysteine (Cys337) and a novel redox motif on the N-terminal. Taken together, we gain insight into the reduction mechanism between PAPS and MjPAPR, thereby suggesting a tentatively proposed reduction mechanism as illustrated in Figure 21. Upon the substrate binding to the active site, the enzyme undergoes a conformational change that brings the redox cysteines (Cys19 and Cys22) comprised in the N-terminal tail directly over the active site. The conformational change also allows the single Cys337 to nucleophilically attack the β-sulfate of the phosphate-sulfur moiety of PAPS. Once the catalytic attack is made, the enzyme-thiosulfonate-intermediate (Cys337-S-$SO3^-$) is formed along with the product, PAP. This is the tentative first step mechanism based on the results from the mutagenesis of C337A. The second half of the reaction mechanism is the release of sulfite in a Trx-dependent manner. Generally, this is the step where Trx nucleophillically attacks the Sγ atom of the intermediate, thus forming a disulfide bond between Trx and the catalytic cysteine of the PAPR [2, 10, 19, 21]. However, in the MjPAPR, the active site is blocked by N-terminal tail containing the redox active cysteines, thereby obstructing the path of the Trx to the intermediate. Instead, the reduced Trx reduces the disulfide bridge of the oxidized Cys19 and Cys22, producing two cysteine thiols. It is not yet conclusive which of the two cysteines attacks the Sγ atom of the intermediate, but for the sake of simplicity we will assume Cys22 is involved in the nucleophilic attack (As shown in Figure 19).

Cys22 now attacks the Sγ atom of the intermediate, displacing the sulfite and forming a disulfide bridge with the Cys337. Finally, the disulfide bridge between the Cys 22 and Cys337 is attacked by the Cys19, thus regenerating the disulfide-linked between the two redox active cysteines. In order to further and solidify our proposed PAPS reduction mechanism in *M. jannaschii*, future studies should focus on the three-dimensional structure of the MjPAPR bound with PAPS and/or Trx.

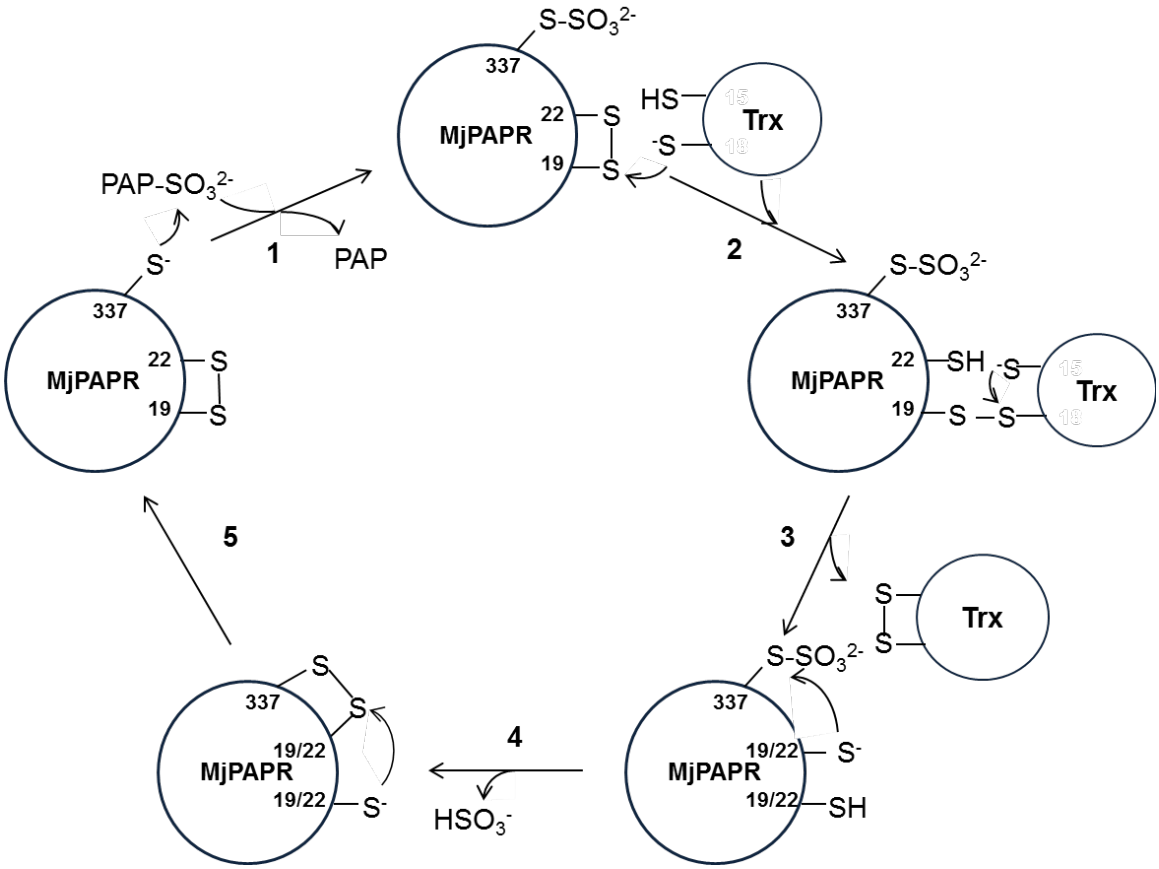

Figure 21. Proposed PAPS reduction mechanism for MjPAPR.

Ecological Implication

M. jannaschii is a methanogenic extremophile that utilizes a carbon source and hydrogen to produce methane to obtain energy [13, 15]. It is found inhabiting the deep-sea hydrothermal vents, which is a 350 ^{0}C anaerobic environment that is rich in sulfide

[31, 32] and its prime oxidation product, sulfate [3, 33]. Sulfate is believed to be present due to the lack of free oxygen in the vent water and the decrease of H_2S concentration with temperature within the vent [33]. It is stated that *M. jannaschii* has the ability to reduce sulfite in a dissimilatory pathway as an alternative, non-methanogenic energy production [3]. Previously, there was a discovery of an APS reductase in *M. jannaschii* [11], which is a key enzyme involved in dissimilatory sulfate reduction pathway [18]. Although previous studies evinces that *M. jannaschii* may utilize sulfate/sulfite in a dissimilatory pathway, the identification of PAPS reductase in *M. jannaschii* suggest that there may be an assimilatory sulfate pathway as well. *M. jannaschii* primarily utilizes methanogenesis to obtain energy [3, 15], which questions the need for a secondary method of producing energy. Sulfur assimilation in archaea has not yet been thoroughly elucidated, but it has been shown that some methanogenic archaea can assimilate sulfur compounds (e.g. sulfate) [16, 34]. Specifically, *M. thermolithotrophicus* and *M. ruminantium* are seen to use sulfate as a sole sulfur source [16]. Due to the methanogenic nature of *M. jannaschii*, methanogenesis serves as a primary source for energy, it appears that there are two viable options for the sulfate inhe the hydrothermal vent: an alternative source for energy via dissimilatory sulfate pathway or a sole sulfur source in the assimilation of sulfate.

Evolutionary Insight on Sulfate Reduction Pathway in Methanogens

The archaean sulfate reduction paradigm was established with the discovery of the F_{420}-dependent sulfite reductase (Fsr) in *M. jannaschii* [3]. This study was able to elucidate how sulfite, an inhibitor of Methyl-CoM reductase, could be reduced by Fsr and coexist with methanogenesis [35]. Fsr utilizes coenzyme F_{420} as an electron carrier [35]

and is found in every methanogens [36]. Furthermore, the discovery of MjAPR supports the existence of a potential sulfate reduction pathway in methanogens [11]. The collective studies provide a thorough insight the intertwined evolutionary history of methanogenesis and sulfate reduction pathway [37].

The existence of sulfate reduction within methanogenic archaea brings forth another question: Is the sulfate reduction pathway assimilatory or dissimilatory? A previous study revealed that sulfite was able to induce the expression of ORF *Mj0870*, which encodes for a sulfite reductase [3]. In addition, the expression of ORF *Mj0973* lead to the discovery a novel APS-reductase, an enzyme associated with dissimilatory sulfate reduction, in *M. jannaschii* [11]. The intertwined relationship of hydrogenotropic methanogenesis and sulfate reduction is believed to be complimentary and essential [37]. The evidence shows that sulfate and sulfite exists in the methanogen's ecosystem [3, 15], and sulfite reduction can detoxify the methyl-CoM reductase and be a source for secondary energy (dissimilatory sulfate reduction) [35, 37].

However, the Fsr found in *M. jannaschii* was stated to have both assimilatory and dissimilatory functions [3, 35]. Hence, the existence of both MjAPR and MjPAPR is very plausible. When the K_m of both MjAPR and MjPAPR are compared, MjAPR seems to have a lower K_m and a higher catalytic efficiency (Table 4). It appears that MjAPR can turnover sulfate as an energy source faster than MjPAPR's ability to assimilate the sulfate. However, both MjAPR and MjPAPR appear to have clear and distinct substrate specificity and functions. Due to the ambiguity of the Fsr and another reported study that identified an assimilatory-type sulfite reductase in late evolving archaea [37], we can

only speculate that there could possibly be a coexistence of both assimilatory and dissimilatory sulfate reduction pathway in *M. jannaschii.*

Table 4. Comparison of Kinetic Parameters of MjAPR and MjPAPR

	K_m(μM)	k_{cat}(1/s)	k_{cat}/ K_m(1/M.s)	Ref (#)
MjAPR	0.29	0.08690	299655	[11]
MjPAPR	15.9	0.08859	5571	

Activities of MjAPR were measured with 1mM Trx as the electron donor.

CHAPTER FIVE

Conclusion

Sulfate assimilation in prokaryotes and eukaryotes has been studied, and it has been unified with a universal mechanism regardless of the differing substrate specificity and presence/lack of iron sulfur cluster. We chose to study the PAPS reductase in *M. jannaschii*, which is the gene product of ORF *Mj0066*, in order to investigate the sulfate assimilation mechanism within archaea. In our study we have discovered a unique enzyme-thiosulfonate intermediate and a novel N-terminus redox site. Hence, we combined our data with the knowledge of the conserved mechanism for sulfonucleotide reduction to postulate a tentative sulfate reduction mechanism for a novel assimilatory sulfate reduction in *M. jannaschii*.

Our study led to paradigm shifting cross road with former ideas regarding methanogens and sulfate reduction. The idea of sulfate reduction and methanogenesis seemed to paradoxical, but previous studies showed evidence of how they can coexist [37]. The previous discovery of MjAPR and the current discovery of MjPAPR now bring a new set of questions. Which pathway is dominant? The kinetic data advocates that dissimilatory sulfate reduction should be dominant. But why would methanogens require a secondary source of energy? Thermodynamic study of MjAPR should be conducted and compared to the midpoint potential of MjPAPR to see which of the two is thermodynamically favorable. Also, the functional ambiguity of the sulfite reductase (Fsr) and the existence of the ORF *M0973* and *Mj0066* may suggest the coexistence of

assimilatory and dissimilatory sulfate reduction pathway. Further study should investigate, in depth, which sulfate reduction pathway methanogens take.

APPENDIX

APPENDIX

Supplementary Figures

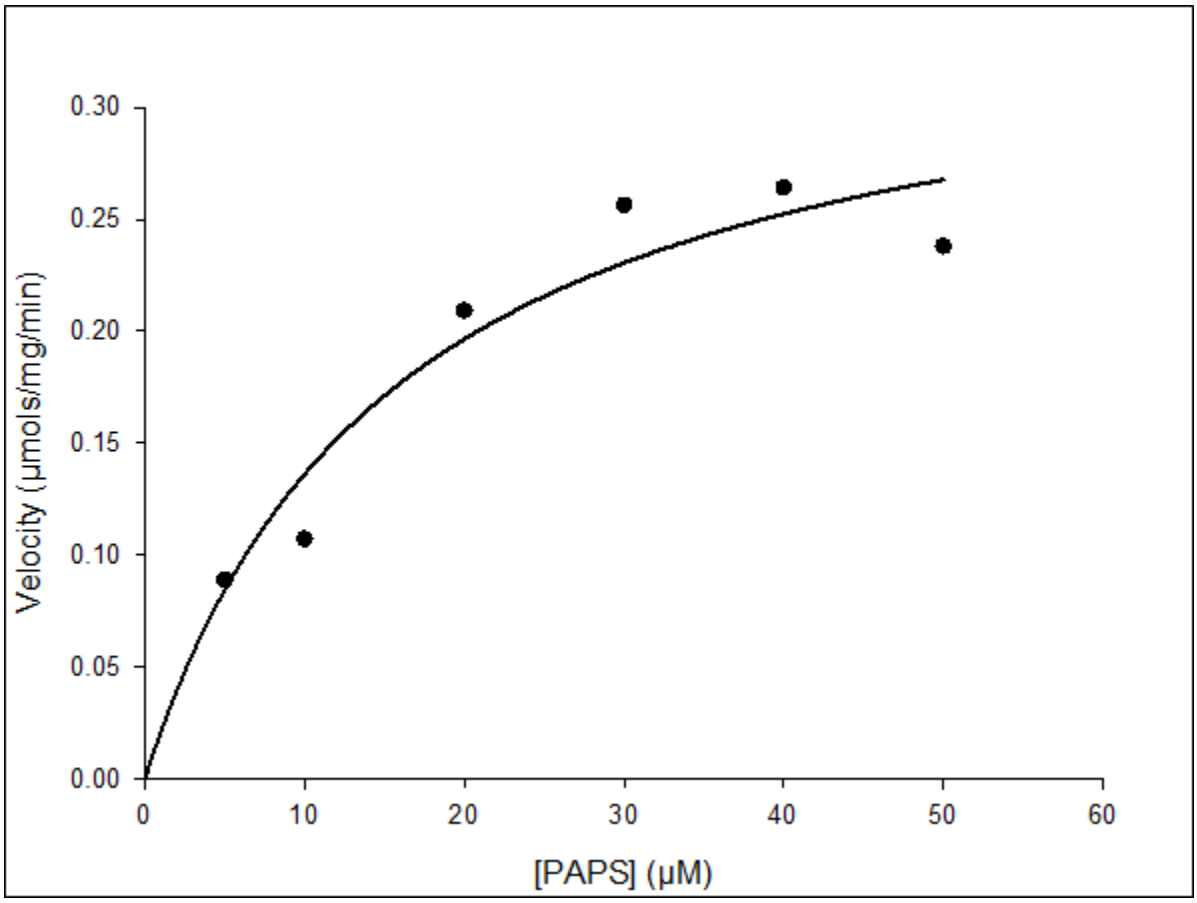

Figure A.1. Michaelis-Menton curve of MjPAPR variant C31A. The K_m and V_{max} for the variant C31A is 15.9 µM and 0.07059 µmol/mg/min, respectively.

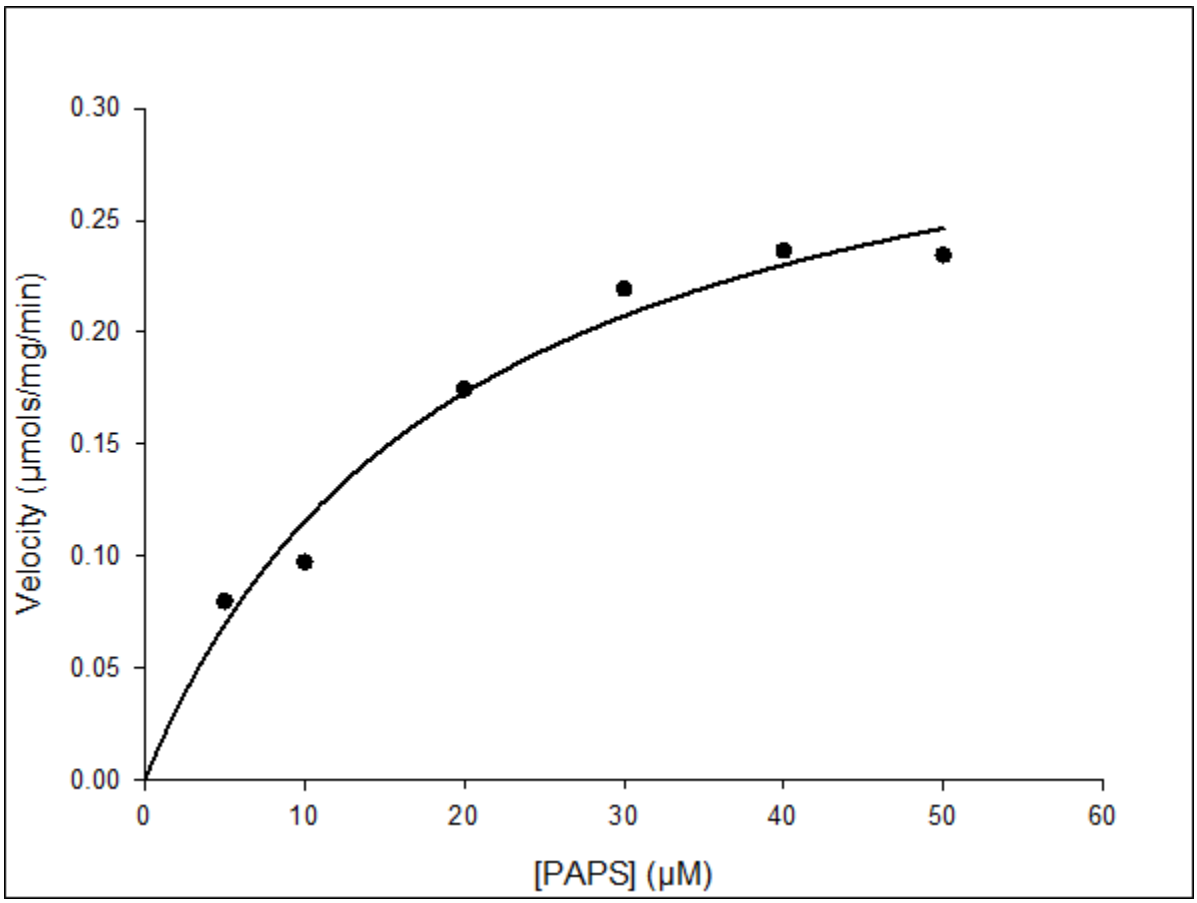

Figure A.2. Michaelis-Menton curve of MjPAPR variant C34A. The K_m and V_{max} for the variant C34A is 19.8 µM and 0.06882 µmol/mg/min, respectively.

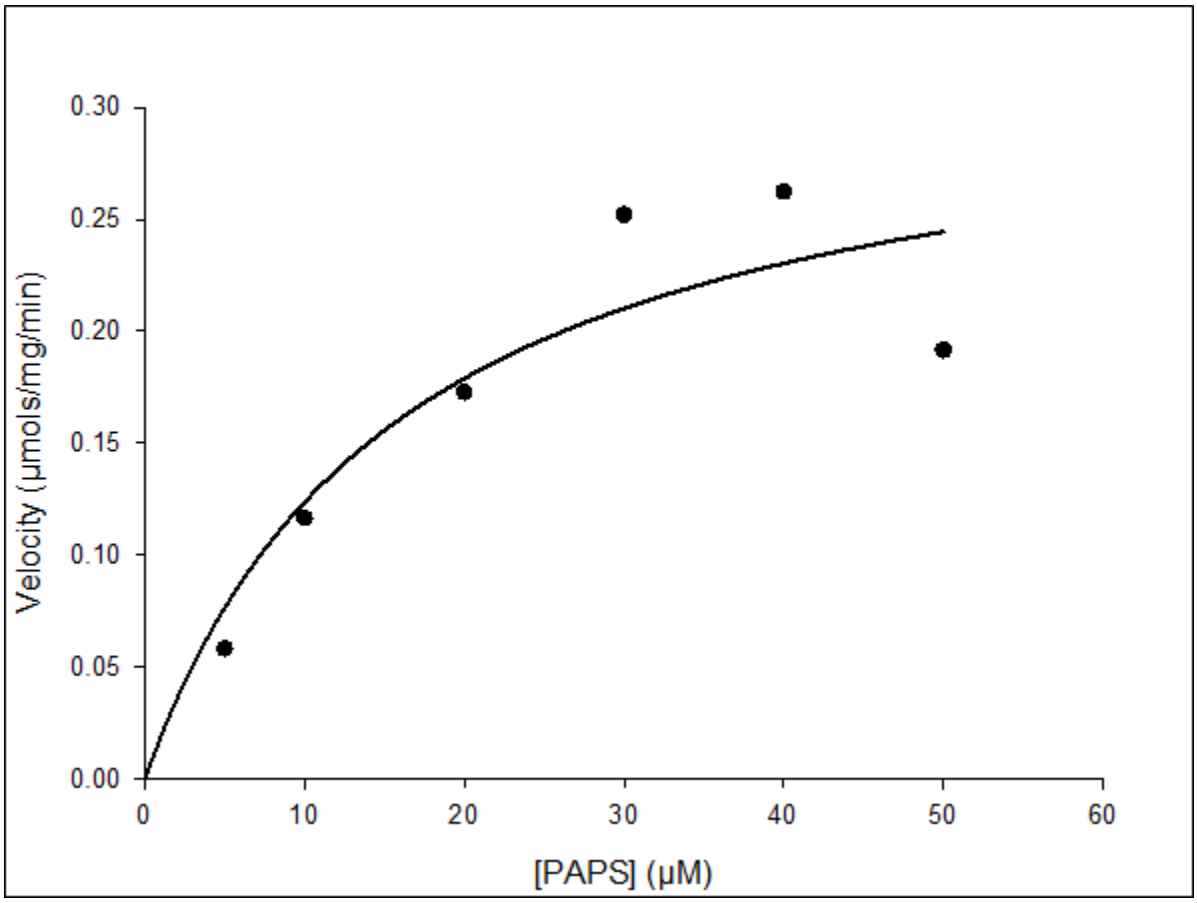

Figure A.3. Michaelis-Menton curve of MjPAPR variant C341A. The K_m and V_{max} for the variant C341A is 16.2 µM and 0.06471 µmol/mg/min, respectively.

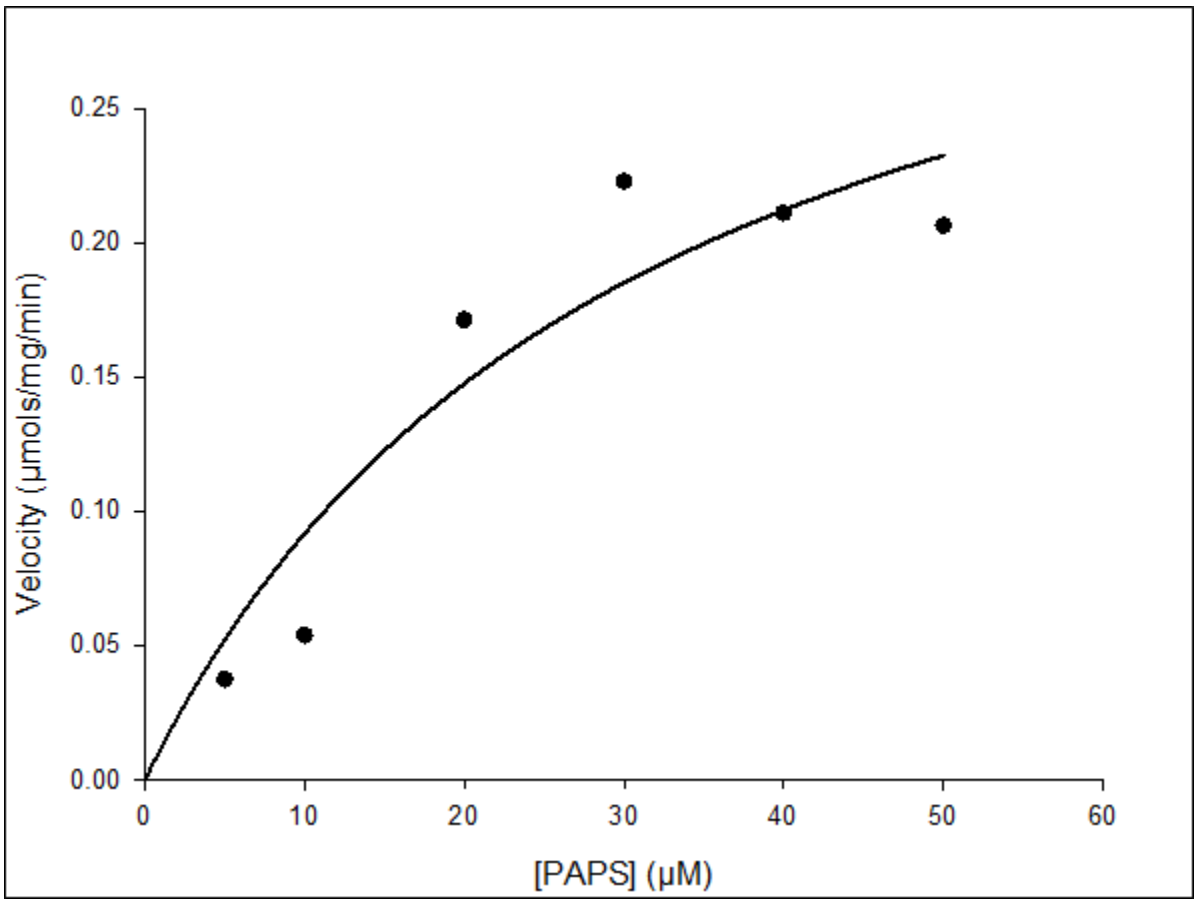

Figure A.4. Michaelis-Menton curve of MjPAPR variant C425A. The K_m and V_{max} for the variant C425A is 31.2 µM and 0.07551 µmol/mg/min, respectively.

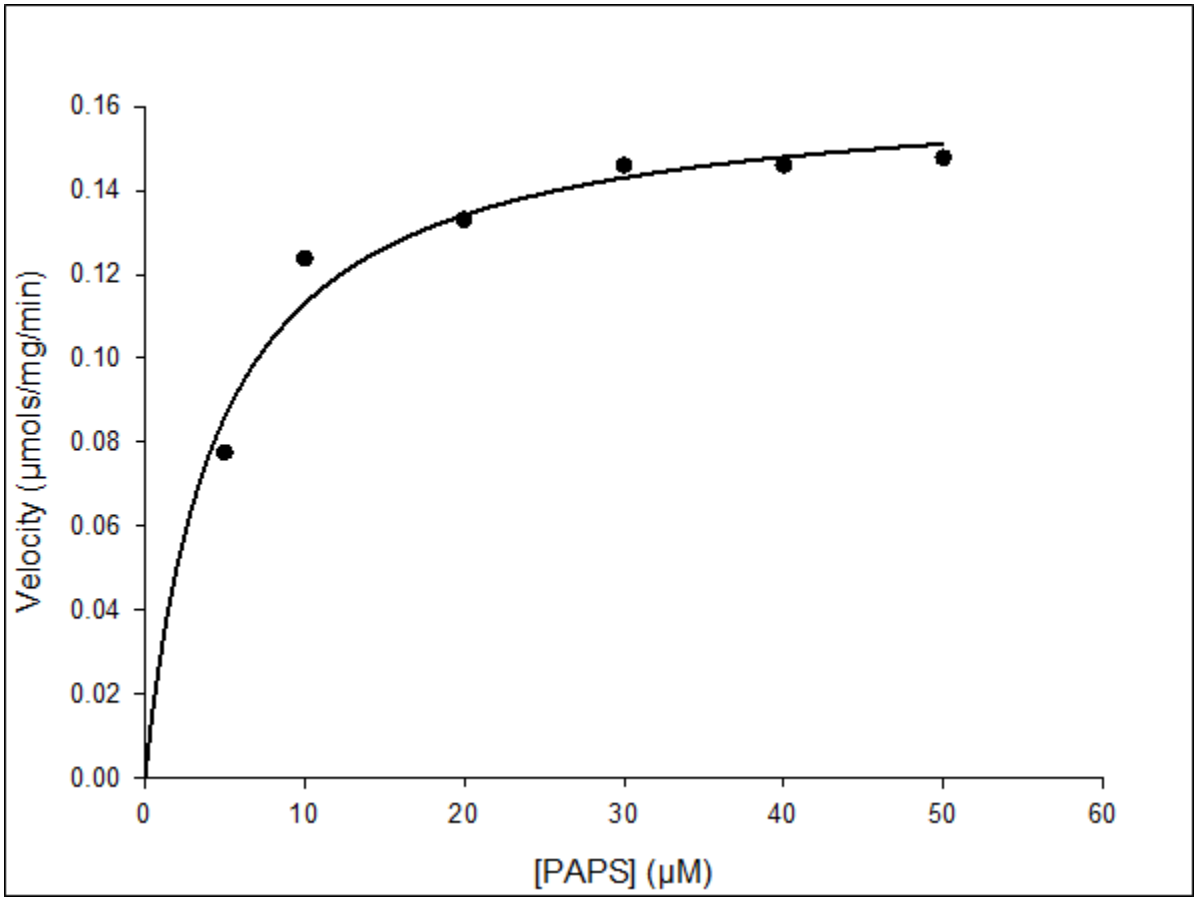

Figure A.5. Michaelis-Menton curve of MjPAPR variant C428A. The K_m and V_{max} for the variant C428A is 4.6 µM and 0.03300 µmol/mg/min, respectively.

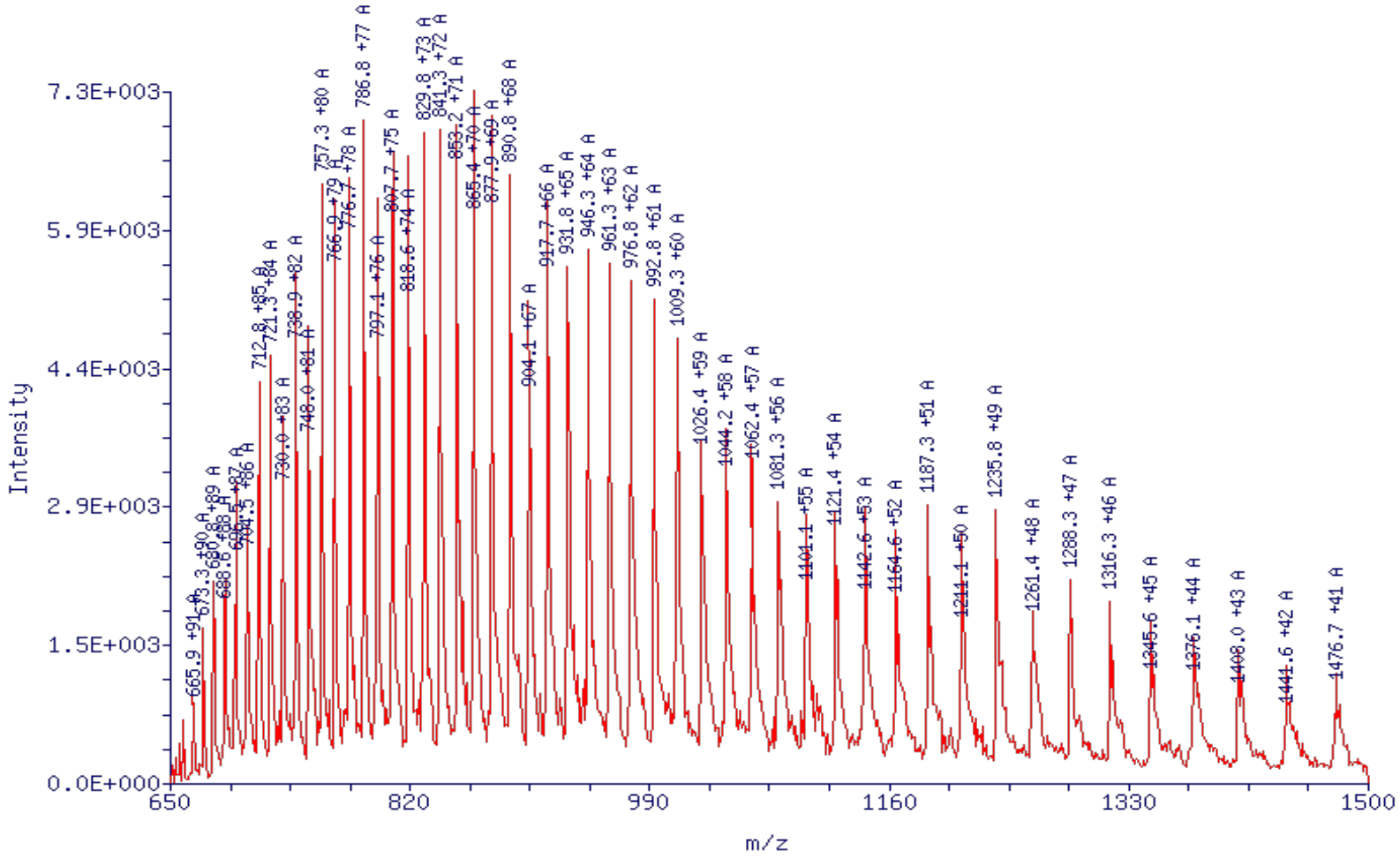

Figure A.6. Mass Spectrum of MjPAPR

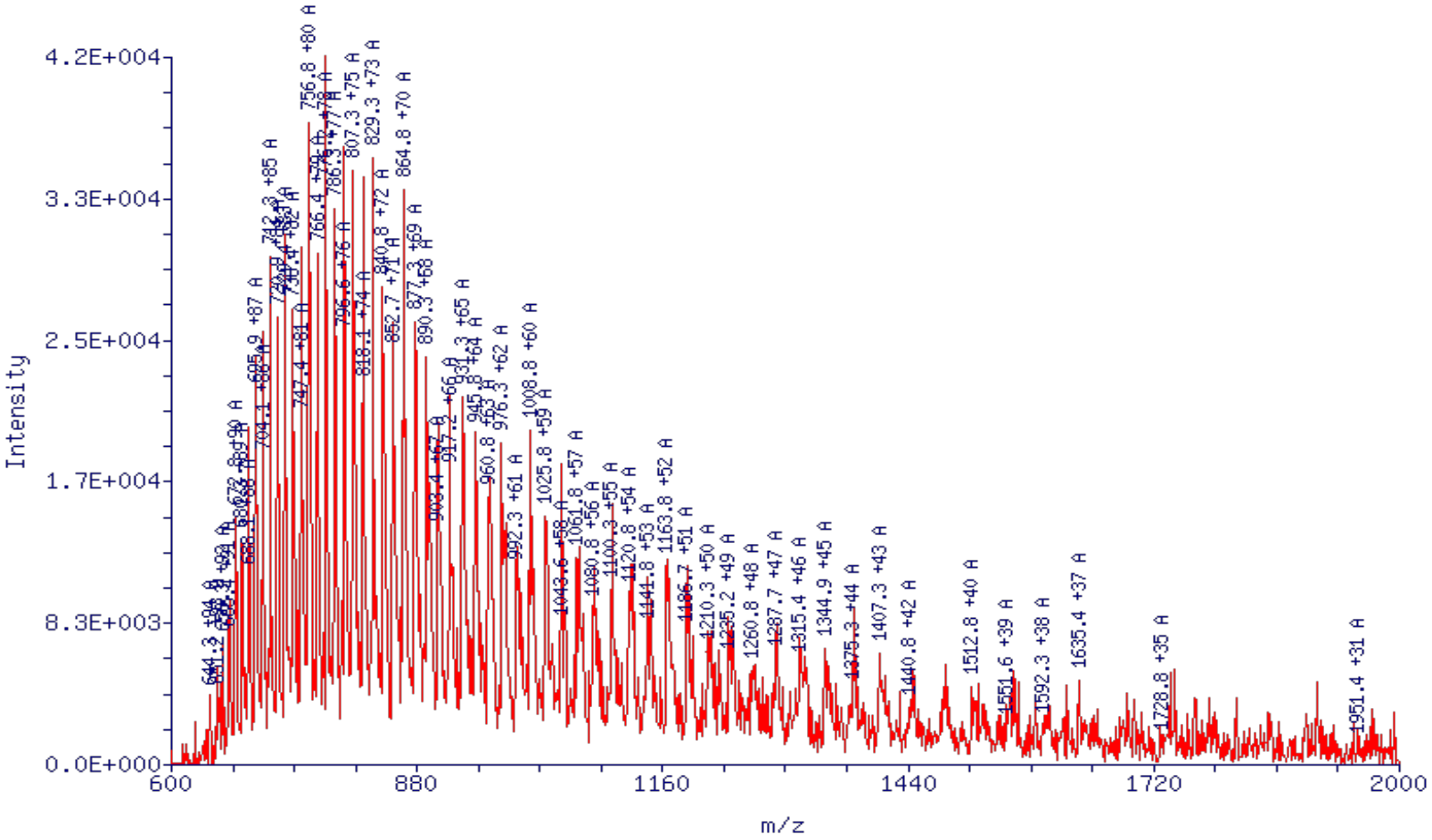

Figure A.7. Mass Spectrum of MjPAPR C19A

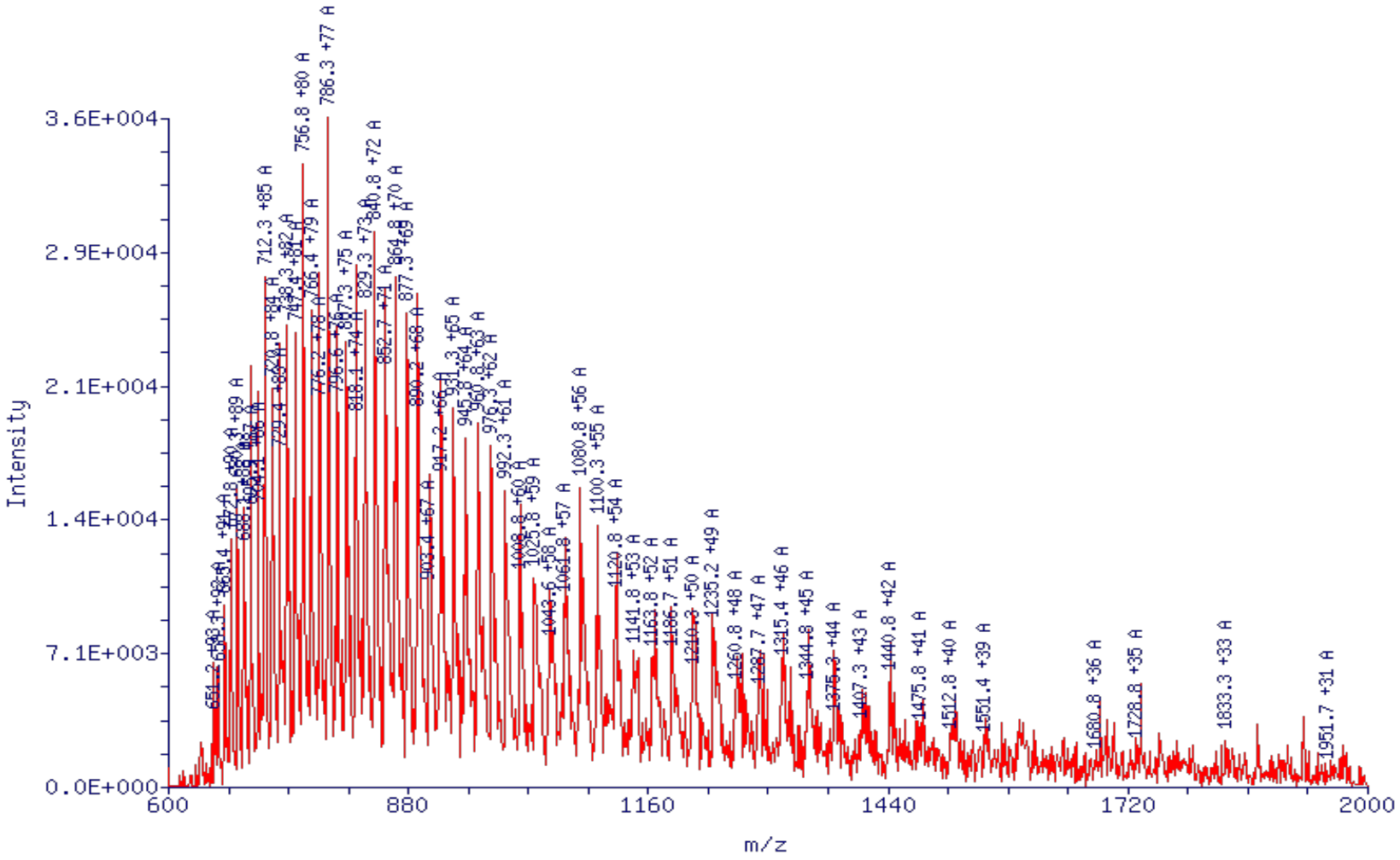

Figure A.8. Mass Spectrum of MjPAPR C22A

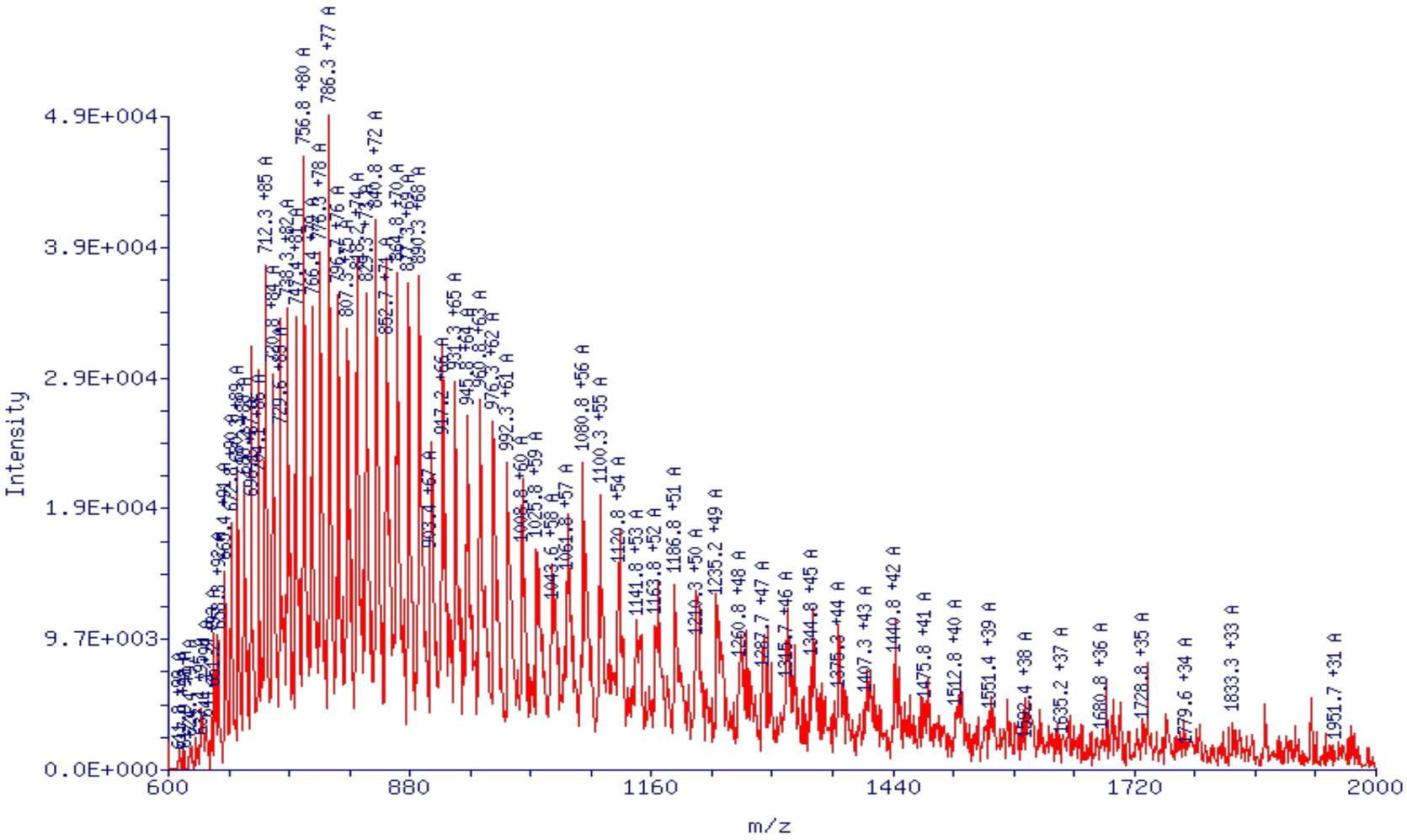

Figure A.9. Mass Spectrum of MjPAPR C337A

REFERENCES

[1] Kopriva S, Fritzemeier K, Wiedemann G, Reski R. The putative moss 3'-phosphoadenosine-5'-phosphosulfate reductase is a novel form of adenosine-5'-phosphosulfate reductase without an iron-sulfur cluster. J Biol Chem 2007;282:22930-22938.

[2] Yu Z, Lemongello D, Segel IH, Fisher AJ. Crystal structure of Saccharomyces cerevisiae 3'-phosphoadenosine-5'-phosphosulfate reductase complexed with adenosine 3',5'-bisphosphate. Biochemistry 2008;47:12777-12786.

[3] Johnson EF, Mukhopadhyay B. A new type of sulfite reductase, a novel coenzyme F420-dependent enzyme, from the methanarchaeon Methanocaldococcus jannaschii. J Biol Chem 2005;280:38776-38786.

[4] Lillig CH, Prior A, Schwenn JD, Aslund F, Ritz D, Vlamis-Gardikas A, Holmgren A. New thioredoxins and glutaredoxins as electron donors of 3'-phosphoadenylylsulfate reductase. J Biol Chem 1999;274:7695-7698.

[5] Bick JA, Dennis JJ, Zylstra GJ, Nowack J, Leustek T. Identification of a new class of 5'-adenylylsulfate (APS) reductases from sulfate-assimilating bacteria. J Bacteriol 2000;182:135-142.

[6] Savage H, Montoya G, Svensson C, Schwenn JD, Sinning I. Crystal structure of phosphoadenylyl sulphate (PAPS) reductase: a new family of adenine nucleotide alpha hydrolases. Structure 1997;5:895-906.

[7] Thauer RK, Jungermann K, Decker K. Energy conservation in chemotrophic anaerobic bacteria. Bacteriol Rev 1977;41:100-180.

[8] Kopriva S, Buchert T, Fritz G, Suter M, Weber M, Benda R, Schaller J, Feller U, Schurmann P, Schunemann V, Trautwein AX, Kroneck PM, Brunold C. Plant adenosine 5'-phosphosulfate reductase is a novel iron-sulfur protein. J Biol Chem 2001;276:42881-42886.

[9] Kim SK, Rahman A, Mason JT, Hirasawa M, Conover RC, Johnson MK, Miginiac-Maslow M, Keryer E, Knaff DB, Leustek T. The interaction of 5'-adenylylsulfate reductase from Pseudomonas aeruginosa with its substrates. Biochim Biophys Acta 2005;1710:103-112.

[10] Chartron J, Shiau C, Stout CD, Carroll KS. 3'-Phosphoadenosine-5'-phosphosulfate reductase in complex with thioredoxin: a structural snapshot in the catalytic cycle. Biochemistry 2007;46:3942-3951.

[11] Lee JS, White E, Kim SG, Schlesinger SR, Lee SY, Kim SK. Discovery of a Novel Adenosine 5'-phosphosulfate (APS) Reductase from the Methanarcheon Methanocaldococcus jannaschii. Process Biochemistry 2011;46:154-161.

[12] Bult CJ, White O, Olsen GJ, Zhou L, Fleischmann RD, Sutton GG, Blake JA, FitzGerald LM, Clayton RA, Gocayne JD, Kerlavage AR, Dougherty BA, Tomb JF, Adams MD, Reich CI, Overbeek R, Kirkness EF, Weinstock KG, Merrick JM, Glodek A, Scott JL, Geoghagen NS, Venter JC. Complete genome sequence of the methanogenic archaeon, Methanococcus jannaschii. Science 1996;273:1058-1073.

[13] Deppenmeier, U. The unique biochemistry of methanogenesis. Progress in Nucleic acid research and molecular biology 2002; 71: 223-282.

[14] Ragsdale, S. W., Becker, D. F. Activation of Methyl-SCoM Reductase to high specific activity after treatment of whole cells with sodium sulfide. *Biochemistry* 1998; 37: 2639-2647.

[15] Horikoshi, K., Grant, W. D. Extremophiles Microbial life in Extreme Environments. Wiley-Liss 1998

[16] Daniels, L., Belay, N., Rajagophol, B. S. Assimilatory reduction of sulfate and sulfite by methanogenic bacteria. Applied and Environmental Microbiology 1986; 51: 703-709

[17] Liu, Y., Beer, L., Whitman, W. B. Methanogens: a window into ancient sulfur metabolism. Trends in Microbiology 2012; 20: 251-258

[18] Peck, H. D. Enzymatic Basis for Assimilatory and dissimliatory sulfate reduction. *Journal of bacteriology* 1961; 82: 933-938.

[19] Chartron J, Shiau C, Stout CD, Carroll KS. 3'-Phosphoadenosine-5'-phosphosulfate reductase in complex with thioredoxin: a structural snapshot in the catalytic cycle. Biochemistry 2007;46:3942-3951.

[20] Bork P, Koonin EV. A P-loop-like motif in a widespread ATP pyrophosphatase domain: implications for the evolution of sequence motifs and enzyme activity. Proteins 1994;20:347-355.

[21] Chartron J, Carroll KS, Shiau C, Gao H, Leary JA, Bertozzi CR, Stout CD. Substrate recognition, protein dynamics, and iron-sulfur cluster in Pseudomonas aeruginosa adenosine 5'-phosphosulfate reductase. J Mol Biol 2006;364:152-169.

[22] Berendt U, Haverkamp T, Prior A, Schwenn JD. Reaction mechanism of thioredoxin: 3'-phospho-adenylylsulfate reductase investigated by site-directed mutagenesis. Eur J Biochem 1995;233:347-356.

[23] Berndt C, Lillig CH, Wollenberg M, Bill E, Mansilla MC, de Mendoza D, Seidler A, Schwenn JD. Characterization and reconstitution of a 4Fe-4S adenylyl sulfate/phosphoadenylyl sulfate reductase from Bacillus subtilis. J Biol Chem 2004;279:7850-7855.

[24] Leustek, T. Identification of a New Class of 5'-Adenylylsulfate (APS) Reductase from Sulfate-Assimilating Bacteria. J. Bacteriol. 2000; 182(1):135-142.

[25] Chakrabarti P. Anion binding sites in protein structures. J Mol Biol 1993;234:463-482.

[26] Harlos K, Vas M, Blake CF. Crystal structure of the binary complex of pig muscle phosphoglycerate kinase and its substrate 3-phospho-D-glycerate. Proteins 1992;12:133-144.

[27] Kim SK, Gomes V, Gao Y, Chandramouli K, Johnson MK, Knaff DB, Leustek T. The two-domain structure of 5'-adenylylsulfate (APS) reductase from Enteromorpha intestinalis is a requirement for efficient APS reductase activity. Biochemistry 2007;46:591-601.

[28] Kim SG, Chi YH, Lee JS, Schlesinger SR, Zabet-Moghaddam M, Chung JS, Knaff DB, Kim ST, Lee SY, Kim SK. Redox properties of a thioredoxin-like Arabidopsis protein, AtTDX. Biochim Biophys Acta 2010;1804:2213-2221.

[29] Holmgren A. Thioredoxin and glutaredoxin systems. J Biol Chem 1989;264:13963-13966.

[30] Berendt U, Haverkamp T, Prior A, Schwenn JD. Reaction mechanism of thioredoxin: 3'-phospho-adenylylsulfate reductase investigated by site-directed mutagenesis. Eur J Biochem 1995;233:347-356.

[31] Jones, W. J., Leigh, J. A., Mayer, F., Woese, C.R., and Wolfe, R. S (1983) Archi. Microbiol. 136, 254-261.

[32] Jannasch, H. W. A novel group of abyssal methanogenic archaebacteria (Methanopyrus) growing at 110°C. Nature. 1989;342:833-834

[33] Jannasch, H. W., Mottl, M. J. Geomicrobiology of deep-sea hydrothermal vents (1985) Science 299: 717-725

[34] Daniels, L. Investigation of mercaptans, organic sulfides, and inorganic sulfur compounds as sulfur sources for the growth of Methanogenic bacteria. Curr. Microbiol. 14:137-144.

[35] Johnson EF, Mukhopadhyay B. Coenzyme F_{420}-dependent sulfite reductase=enabled sulfite detoxification and use of sulfite as a sole sulfur source by *Methanococcus maripaldudis.* App Environ Microbiol. 2008;74:3591-3595.

[36] DiMarco AA, Bobik TA, Wolfe RS. Unusual coenzymes of methanogenesis. Annu Rev Biochem. 1990;59:355-394.

[37] Dwi, S., Biswarup, M. An Intertwined Evolutionary History of Methanogenic Archaea and Sulfate Reduction. PLOS one. 2012;(Vol 7)9:e45313